Genetic relationship between greisenization and Sn-W mineralizations in vein and greisen deposits: Insights from the Panasqueira deposit (Portugal)

Gaëtan Launay, Stanislas Sizaret, Philippe Lach, Jérémie Melleton, Eric Gloaguen, Marc Poujol

BSGF - Earth Sciences Bulletin 2021, 192, 2
© G. Launay *et al.*, Published by EDP Sciences 2021
https://doi.org/10.1051/bsgf/2020046

Special Issue Minéralisations périgranitiques, ed. E. Marcoux

BSGF Earth Sciences Bulletin
Available online at:
www.bsgf.fr

OPEN ACCESS

Genetic relationship between greisenization and Sn-W mineralizations in vein and greisen deposits: Insights from the Panasqueira deposit (Portugal)

Gaëtan Launay[1,*], Stanislas Sizaret[2], Philippe Lach[3], Jérémie Melleton[3], Éric Gloaguen[2,3] and Marc Poujol[4]

[1] Department of Earth Sciences, Laurentian University, Sudbury, Ontario P3E 2C6, Canada
[2] ISTO, UMR7327, Université d'Orléans, CNRS, BRGM, F-45071 Orléans, France
[3] BRGM, F-45060 Orléans, France
[4] Géosciences Rennes, UMR CNRS 6118, Université de Rennes 1, OSUR, Campus de Beaulieu, 35042 Rennes, France

Received: 7 October 2020 / Accepted: 16 December 2020

Abstract – The W-Sn Panasqueira ore deposit is a magmatic-hydrothermal system, which includes a high grade quartz-vein type mineralization and underneath disseminated greisen-type mineralization located in the upper part of a two-mica granite. We investigate genetic and chronological relationships between greisenization of the Panasqueira granite and the formation of ore-bearing quartz veins by monitoring major and trace elements variations in quartz-muscovite assemblages composing the two-mica granite, greisen and ore-bearing quartz veins. Greisen is marked by an overall depletion in Mg, Ti, Ca, Na, Ba, Sr, REE and enrichment in Fe, Li, Rb, Cs, Sn, W that reflect the breakdown of feldspars and biotite and implication of W-Sn-bearing fluids during greisenization. Muscovite from greisen and mineralized quartz veins are enriched in granophile elements (F, Rb, Cs, Li, Sn, W and Zn) compared to magmatic muscovite from the two-mica granite. Trace elements contents in quartz depict evolutionary trends with progressive enrichment in Ge and B and depletion in Al, Ti and Li between magmatic and hydrothermal quartz that emphasize the progressive evolution and cooling of the magmatic-hydrothermal system of Panasqueira. Multivariate statistical approach applied on quartz and muscovite data demonstrates similarities in composition between quartz and muscovite from greisen with those composing ore-bearing quartz veins. These similarities suggest that greisenization and the formation of mineralized veins result from the same hydrothermal event and derived from the same source of hydrothermal fluids. Apatite from greisen and quartz vein yielded respectively U-Pb ages of 292 ± 10 Ma and 295 ± 5 Ma confirming that greisenization and the formation of mineralized veins occurred roughly at the same time. These ages also overlap with the cooling age of the Panasqueira granite (296 ± 4 Ma), indicating a temporal and genetic link between greisenization, W-Sn mineralization and the granite crystallization. Temperatures of the magmatic-hydrothermal system constrained by Ti-in quartz thermometry depicts a cooling trend from magmatic quartz of granite (700–600 °C) to hydrothermal quartz of greisen (500–400 °C) and veins (450–350 °C). These results provide evidences that greisenization and the formation of W-Sn bearing quartz veins occurred at the magmatic-hydrothermal transition, during which orthomagmatic fluids rich in volatils, incompatible elements and metals (W and Sn) were exsolved at the final stage of solidification of the Panasqueira two-mica granite.

Keywords: Vein and greisen Sn-W deposits / Panasqueira / Muscovite chemistry / Quartz trace chemistry / U-Pb dating of Apatite / magmatic-hydrothermal evolution

Résumé – Relations génétiques entre greisenisation et minéralisation à Sn-W dans les gisements de type veines et greisen : nouvelles contraintes du gisement de Panasqueira (Portugal). Le gisement à W-Sn de Panasqueira (Portugal) est un système magmatique-hydrothermal de type veine et greisen dont la minéralisation se présente principalement sous la forme d'un réseau dense de veines à quartz-wolframite. Ce gisement comprend également des minéralisations disséminées à faibles teneurs au sein d'un apex granitique greisenisé. Cette étude vise à contraindre les relations génétiques et chronologiques entre la

*Corresponding author: glaunay@laurentian.ca

greisenisation du granite de Panasqueira et la formation des veines à W-Sn en s'appuyant sur la composition géochimique des assemblages à quartz-muscovite composant le granite, le greisen et les veines minéralisées de Panasqueira. Le greisen se caractérise par un appauvrissement en Mg, Ti, Ca, Na, Ba, Sr, REE et un enrichissement en Fe, Li, Rb, Cs, Sn, W reflétant (i) l'altération des feldspaths et de la biotite et (ii) l'implication des fluides porteurs de la minéralisation à W-Sn lors de la greisenisation. La muscovite composant le greisen ainsi que les veines de quartz minéralisées sont enrichies en éléments granophiles (F, Rb, Cs, Li, Sn, W et Zn) par rapport à la muscovite magmatique composant le granite. La composition en éléments trace des différentes générations de quartz magmatiques et hydrothermaux montre un enrichissement progressif en Ge et B et un appauvrissement en Al, Ti et Li entre quartz magmatiques et hydrothermaux. L'application d'approches statistiques multivariées démontre que les compositions géochimiques des quartz et des muscovites composant le greisen et les veines minéralisées sont similaires. Ces similarités suggèrent que la greisenisation et la formation des veines minéralisées de Panasqueira résultent d'un même événement hydrothermal et impliquent la même source de fluides. Les apatites présentes au sein du greisen et des veines minéralisées se caractérisent respectivement par des âges U-Pb de 292 ± 10 Ma et 295 ± 5 Ma confirmant que la greisenisation est contemporaine à la formation de veines minéralisées. Ces âges sont également compatibles avec l'âge de refroidissement du granite (296 ± 4 Ma) indiquant un lien temporel et génétique entre la greisenisation, la minéralisation à W-Sn et la cristallisation du granite de Panasqueira. Les températures du système magmatique-hydrothermal contraintes à partir du géothermomètre TitaniQ (Ti-Quartz) montrent un refroidissement progressif des quartz magmatiques du granite (700–600 °C) vers les quartz hydrothermaux composant le greisen (500–400 °C) et les veines minéralisées (450–350 °C). Ces résultats indiquent que la greisenisation et la formation des veines a W-Sn de Panasqueira se sont produites lors de la transition magmatique-hydrothermale, au cours de laquelle des fluides d'origine magmatique riches en volatils, en éléments incompatibles et en métaux (W et Sn) ont été expulses lors de la cristallisation du granite de Panasqueira.

Mots clés : Gisements de type veines et greisen / Panasqueira / Géochimie de la muscovite / Éléments en trace dans les quartz / Datation U-Pb sur Apatite / Évolution magmatique-hydrothermale

1 Introduction

The vein and greisen tin-tungsten (Sn-W) deposits supply an important part of the world Sn and W (Kotlyar *et al.*, 1995; Robb, 2005; Werner *et al.*, 2014). This type of deposit is generally developed at the edge of granite cupolas that constitute the apical parts of larger polyphased granite intrusions occurring at depth (Stemprok, 1987; Pollard *et al.*, 1988; Lehmann, 1990; Pirajno, 1992; Černý *et al.*, 2005; Stemprok *et al.*, 2005). The formation of these deposits involves continuum of magmatic-hydrothermal processes and implies the transfer and the focusing of a large amount of mineralizing fluids (Pirajno, 1992; Černý *et al.*, 2005; Dolejs, 2015). These deposits generally include (i) a disseminated mineralization within a massive greisen characterized by low grade and high tonnage and (ii) W-Sn bearing mineralized quartz veins usually characterized by high grade and low tonnage (Taylor, 1979; Taylor and Pollard, 1988; Lehmann, 1990; Mlynarczyk *et al.*, 2002). Despite evident spatial relationships between greisen and vein mineralizations, the detailed processes involved and the timing of hydrothermal events related to the formation of these two types of ore bodies remain poorly constrained. Futhermore, most studies are mainly focused on formation of only one these type and comparison between greisen and mineralized veins are scarce (Launay *et al.*, 2018). However, a recent fluid inclusions study performed by Korges *et al.* (2018) in the Zinnwald Sn-W vein-and-greisen deposit (Erzebirge, at the Czech Republic-Germany boundary) suggests that greisenization and the formation of mineralized veins could be contemporaneous and related to the exsolution and the boiling of a single Sn-W-rich magmatic fluids.

Quartz-muscovite assemblage is common both in greisen and in their associated mineralized veins: Panasqueira, Portugal (Kelly and Rye, 1979; Neiva, 1987; Neiva *et al.*, 2007), Piotang, China (Legros *et al.*, 2016, 2018), Cinovec, Erzgebirge (Breiter *et al.*, 2017; Müller *et al.*, 2018; Breiter *et al.*, 2019), Cligga Head, Cornwall (Sanderson *et al.*, 2008) and Echassieres district, France (Monnier *et al.*, 2018, 2019). These minerals are able to incorporate a wide range of various trace elements that can be used as indicators of the evolution of magmatic-hydrothermal systems (Miller *et al.*, 1981; Speer, 1984; Monier *et al.*, 1984; Neiva, 1987; Tischendorf *et al.*, 1997; Gomes and Neiva, 2000; Legros *et al.*, 2016, 2018; Breiter *et al.*, 2017; Müller *et al.*, 2018; Michaud *et al.*, 2020). The incorporation of elements in mica is controlled by the crystallization temperature (Monier and Robert, 1986), the oxygen fugacity (Pichavant *et al.*, 2016) and their abundance in the source melt-fluids from which mica have crystallized. Consequently, compositional variations observed between different generations of muscovite composing magmatic-hydrothermal systems permit to (i) trace the cooling of the system; (ii) highlight changes in fO_2; (iii) identify and distinguish magmatic and hydrothermal processes and (iv) constrain the chemical signature of fluid(s) involved in hydrothermal processes (Alfonso *et al.*, 2003; Hulsbosch *et al.*, 2014; Dostal *et al.*, 2015; Legros *et al.*, 2016, 2018; Van Daele *et al.*, 2018; Kaeter *et al.*, 2018).

Quartz is omnipresent in hydrothermal and magmatic environments. It is relatively resistant to post-crystallization alteration and able to incorporate a wide range of trace elements that can be used as a genetic pathfinder to track magmatic and hydrothermal processes (Monecke *et al.*, 2002; Götze *et al.*, 2004; Breiter *et al.*, 2017; Monnier *et al.*, 2018; Müller *et al.*, 2018). The concentrations of these trace elements are generally controlled by (i) their abundances in the parental

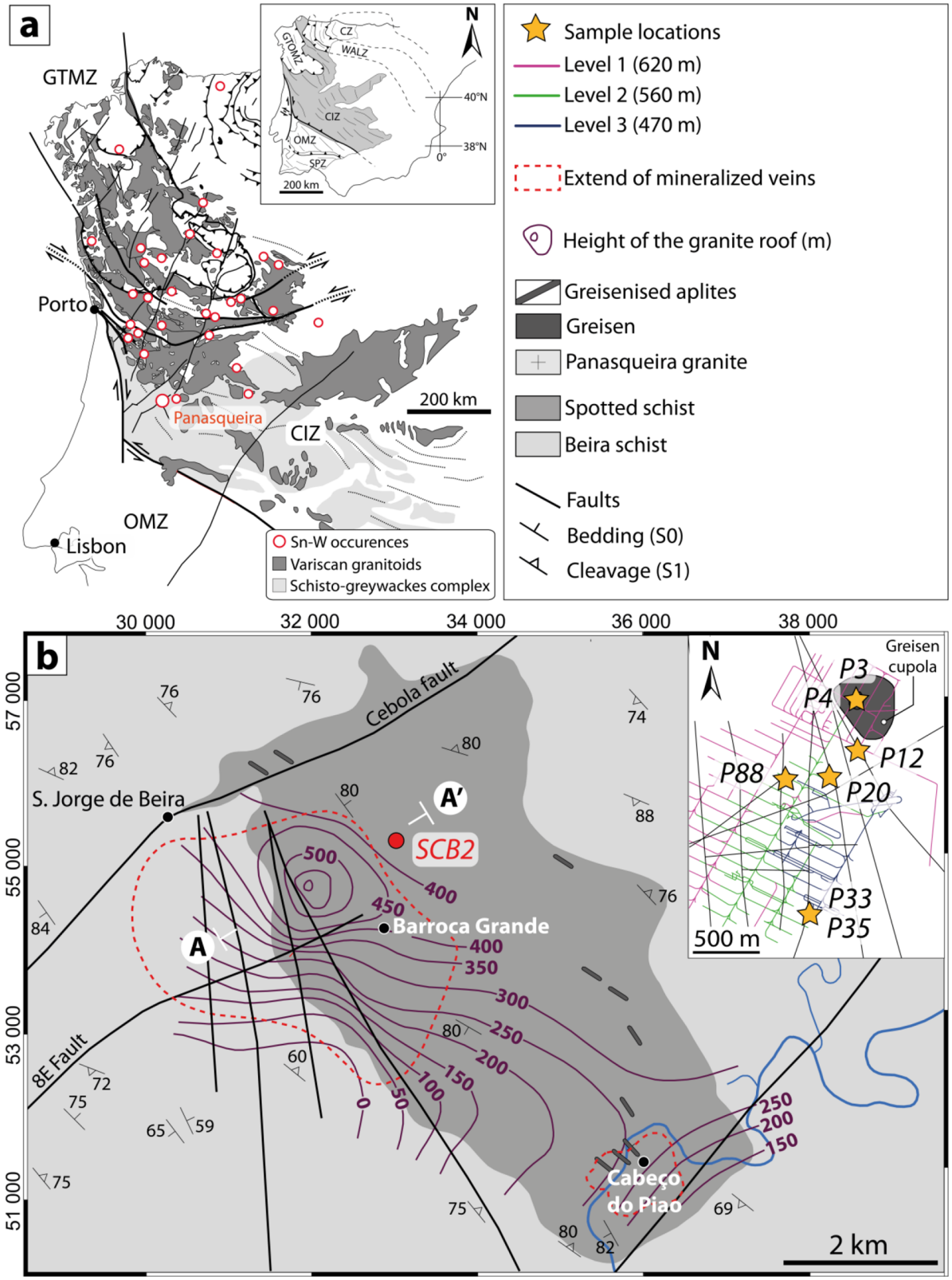

Fig. 1. (a) Tectono-metamorphic map of the Central Iberian Zone displaying spatial relationship between Sn-W occurrences and Variscan granitoids. CZ: Cantabrian Zone; WALZ: West Asturian-Leonese Zone; GTMZ: Galicia Tràs-os-Montes Zone; CIZ: Central Iberian Zone; OMZ: Ossa-Morena Zone and SPZ: South Portuguese Zone (Julivert *et al.*, 1972). (b) Geological map of the Panasqueira district showing the lateral extent of the non-outcropping granite intrusion and the mineralized vein system (modified from Launay, 2019). Projected lat./lon. coordinates, ETRS89 TM6.

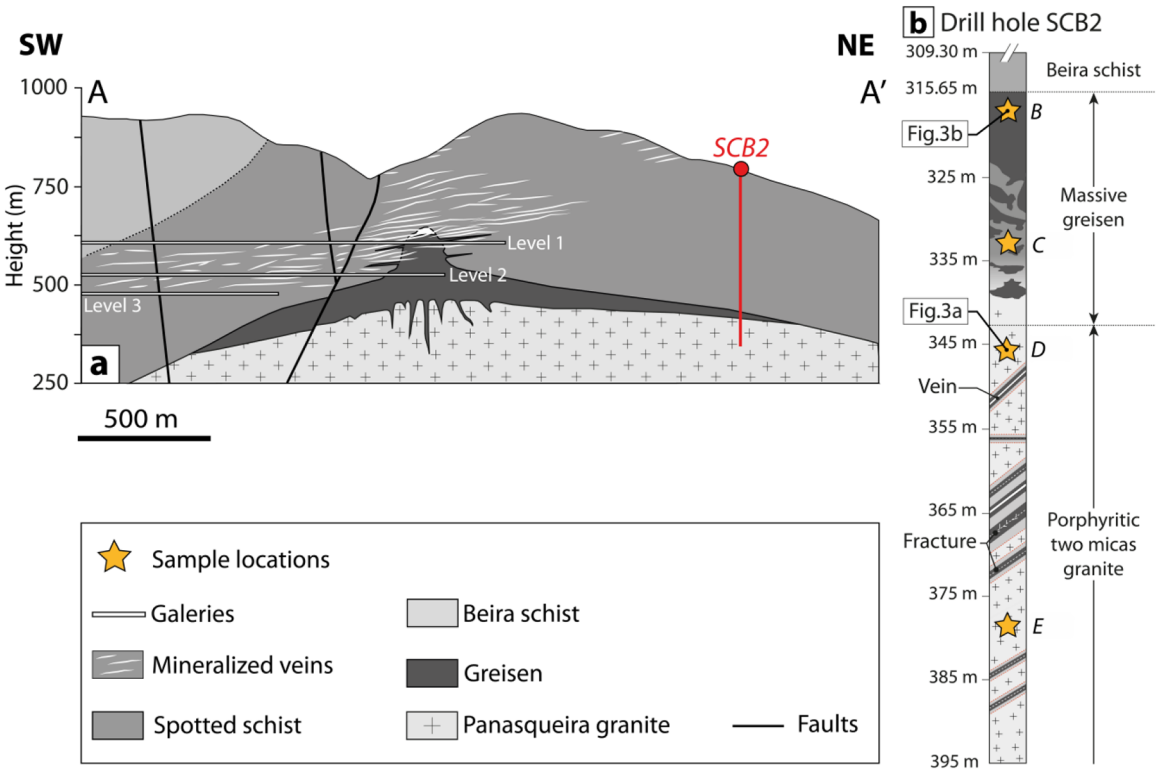

Fig. 2. (a) Geological cross section (A-A') displaying the relationship between greisen (in the top of the intrusive body) and the mineralized vein network. (b) Drill hole SCB2 displaying the vertical zoning of the greisenization of the Panasqueira two mica granite (Location of the drill hole is displayed on the geological map and on the cross-section) (modified from Launay, 2019).

melt and hydrothermal fluids, (ii) partitioning of these elements between co-genetic minerals, (iii) physicochemical conditions and (iv) pressure and temperature conditions (Gurbanov *et al.*, 1999; Larsen *et al.*, 2004; Jacamon and Larsen, 2009; Thomas *et al.*, 2010). Recent studies have demonstrated that Ti content in quartz is generally correlated to the temperature conditions (Thomas *et al.*, 2010; Huang and Audétat, 2012), while the evolution of the Al, Ge and Li permit generally to highlight the melt differentiation induced by fractionated crystallization (Jacamon and Larsen, 2009). Trace element content in quartz is also commonly used to track the magmatic-hydrothermal processes in cases of deposits related to magmatic intrusions (Müller *et al.*, 2002; Breiter *et al.*, 2005, 2012; Rusk, 2012; Müller *et al.*, 2018; Monnier *et al.*, 2018). Recently, analysis of trace elements contents in quartz combined with innovative multivariate statistical analysis of quartz signatures demonstrated in the case of the Beauvoir deposit that greisenization and the formation of proximal Nb-Ta-Sn-W and distal Sb veins could derive from the same hydrothermal fluid (Monnier *et al.*, 2018).

In the following, we investigate genetic and chronological relationships between greisenization and the formation of mineralized veins of the world-class W-Sn-(Cu) Panasqueira ore deposit (Portugal) (Thadeu, 1951; Kelly and Rye, 1979; Polya, 1989; Polya *et al.*, 2000; Foxford *et al.*, 2000; Lecumberri-Sanchez *et al.*, 2017; Codeço *et al.*, 2017, 2019; Launay *et al.*, 2018; Launay, 2019; Carocci *et al.*, 2018). We applied a complete petrological and geochemical study dealing with (i) description of the whole-rock geochemical changes related to the greisenizaton of the Panasqueira granite, and (ii) *in-situ* chemical analyses of major and trace elements in muscovite and quartz composing granite, greisen and the ore-bearing quartz veins. Signatures of the differents populations of quartz and muscovite were then deciphered on the base of principal component analysis (PCA) and permutational multivariate analysis of variance (PERMANOVA). These two statistical approaches permit to (i) identify correlations and behaviours of elements and (ii) decipher the statistical similarities in element concentrations between the different populations of quartz and muscovite.

In addition, new U-Pb dating of magmatic and hydrothermal apatite allows constraining the chronology between the granite cooling, the greisenization and the formation of mineralized veins. Based on the analysis of these various results, we discuss the signature and the origin of fluids responsible of greisenization and the formation of the W-Sn mineralized veins. Finally, we propose a conceptual model describing the genetic relationship between the granite cooling, greisenization and the formation of the mineralized veins of Panasqueira.

2 Geology of the W-Sn-(Cu) Panasqueira deposit

2.1 Geological setting

The W-Sn-(Cu) Panasqueira ore deposit is located in the Central Iberian Zone (CIZ) that covers the middle part of the Iberian Variscan Belt (Julivert *et al.*, 1972) (Fig. 1a). This tectono-metamorphic zone is composed of a thick (8–11 km) monotonous Neoproterozoic schisto-greywacke

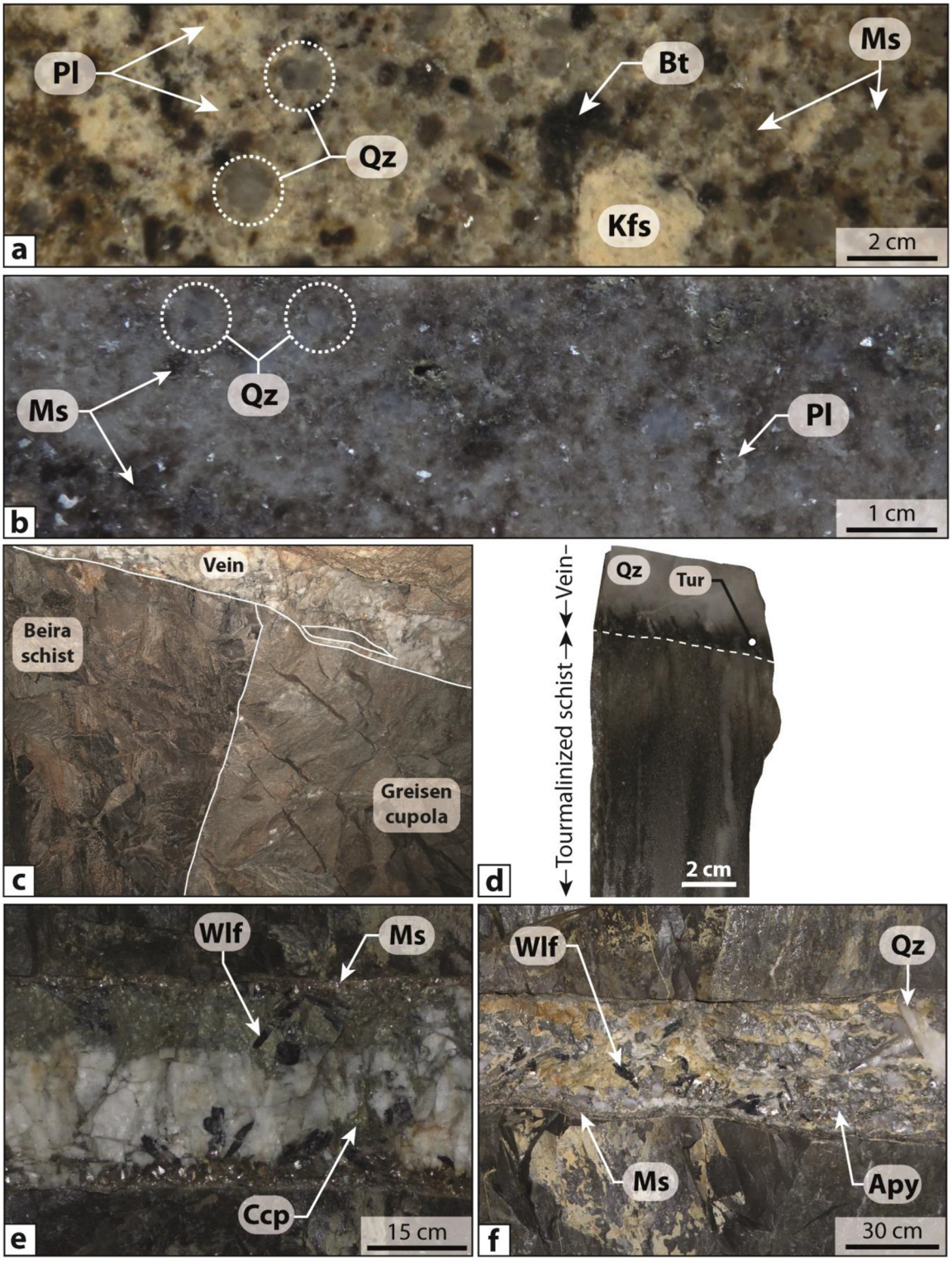

Fig. 3. Textural and mineralogical characteristics of (a) the Panasqueira two-mica granite and (b) greisen in the drill hole SCB2. (c) Contact between the greisen cupola and the metasedimentary host rock. A mineralized quartz vein crosscut this contact. (d) Quartz-tourmaline veinlet characteristic of the QTS mineralization stage. (e) Typical quartz-muscovite vein with wolframite mineralization. Muscovite forms fringes along the schist-vein contacts. (e) Geodic vein displaying euhedral quartz and wolframite nugget infilling vugs between quartz crystals. Note that vugs were also infilled by sulfphides and carbonates during the late mineralization stages. Abbreviations from Whitney and Evans (2010) Apy: Arsenopyrite, Bt: Biotite, Ccp: Chalcopyrite, Kfs: K-feldspar, Ms: Muscovite, Pl: Plagioclase, Qz: Quartz, Wlf: Wolframite.

sequence (*e.g.* Villaseca *et al.*, 2014) unconformably overlain by a lower palaeozoic sequence. The CIZ consists of numerous granitic intrusions mainly emplaced during the latest stages of the Variscan orogeny (Dias *et al.*, 1998; Castro *et al.*, 2002). The CIZ is particularly rich in Sn-W deposits and indices (Vilas *et al.*, 1990), whose formation is related to the magmatic-hydrothermal processes induced by the emplacement of this large volume of granitic bodies (Fig. 1a). These deposits comprise mostly vein and greisen mineralized systems like Regoufe, Gois and Panasqueira, which were/are mainly exploited for the W mineralization.

The W-Sn-(Cu) Panasqueira deposit belongs to the Beira Baixa province located in the South of the Serra da Estrela granitic Massif. This region is largely composed of schist greywacke sequence affected by tight and upright folds and by a low grade greenschist metamorphism during the Variscan orogeny (Azor *et al.*, 2019). The presence of spotted schist delineates a thermal metamorphism aureole, which highlights the presence of a non-outcropping granitic intrusion at depth (Clark, 1964; Kelly and Rye, 1979; Bussink, 1984) (Fig. 1b). The surface distribution of spotted schist, the drill holes distributed over the Panasqueira district and a gravimetric survey show that this granite is characterized by an elongated shape in the NW-SE direction (7.5 × 4.5 km) for a thickness not exceeding 2 km (Fig. 1b) (Thadeu, 1951; Clark, 1964; Kelly and Rye 1979; Hebblethwaite and Antao, 1982; Ribeiro, 2017). The granite's roof dips gently to the NE in the northeastern part and steeply to the SW in the southwestern part of the intrusion (Figs. 1b and 2a). Greisenized apex of the granite is crosscut by the underground mining works (Fig. 2a). The economic W-Sn mineralization consists of a dense swarm of sub-horizontal quartz veins mostly hosted by the metasedimentary host rock (Beira schist).

2.2 The greisen system of Panasqueira

In drill hole the granite intrusion of Panasqueira exhibits a strong vertical zoning of alteration, which increases progressively up to the granite's roof (Fig. 2b) (Launay, 2019). The deeper part of this intrusion is porphyritic two-mica granite composed of K-feldspar phenocryst, albite, muscovite, biotite and snowball-textured quartz (Figs. 2b and 3a). Accessory minerals include zircon, apatites and Fe-Ti oxides. The greisen alteration can be locally observed as narrow alteration halos around fractures and mineralized veinlets (Fig. 2b) (Launay, 2019).

The top of the intrusion exhibits a thick massive greisen (up to 30 m in drill hole) resulting from an intense fluid-rock interaction which affected the underlying two-mica granite (Fig. 2). The cupola (Level 1 and Level 530 of the mine) and granite aplites occuring at the top of the granite intrusion were also entirely converted into greisen and exhibit the same texture and mineral assemblage observed in drill hole. This greisen is marked by the total breakdown of feldspars and biotite, which were replaced by a medium- to coarse-grained quartz-muscovite assemblage (Fig. 3b) (Bussink, 1984; Neiva, 1987; Launay, 2019). As highlighted in Figure 3b, snowball-textured quartz composing the two-mica granite was partially conserved in greisen during the hydrothermal alteration. Apatite, rutile, cassiterite, scarce wolframite, columbo-tantalite and sulfides (chalcopyrite, sphalerite, pyrite and arsenopyrite) occur as accessory minerals disseminated in the greisen. Sulfides, cassiterite and scarce wolframite infilled partially the pores observed in the greisen (Launay, 2019) and can be associated with euhedral quartz in large pockets. Flat-dipping mineralized veins can be also observed within the greisen cupola (Fig. 3c). These veins, which crosscut the sharp contact between the cupola and the metasedimentary host rock (Fig. 3c), exhibit the same paragenesis (*i.e.* muscovite, quartz wolframite and sulfides) than mineralized veins present in the metasedimentary host rocks.

2.3 The mineralized vein swarm

The W-Sn-(Cu) mineralization of Panasqueira is hosted by a dense network of low-dipping quartz veins crosscutting the vertical foliation planes of the Beira schist. This vein network defines an ore zone centred on the greisen cupola and connected with it at depth (Figs. 1b and 2a). This ore zone extends over an area of about 6 km^2 for a depth extension reaching 500 m (Polya *et al.*, 2000; Wheeler, 2015). The veins have recorded a complex history involving different type of mineralization: an early W-Sn stage and a late sulfide (Cu) mineralization event. The complex paragenetic sequence of veins was described in detail by Kelly and Rye (1979) improved by Foxford *et al.* (1991, 2000) and Polya *et al.* (2000). At least five mineralization stages are recognized in the veins: the Quartz-Tourmaline (QTS) stage, the Main Oxide Silicate Stage (MOSS), the Main Sulfide Stage (MSS), the Pyrrhotite Alteration Stage (PAS) and the Late Carbonate Stage (LCS). The two earliest mineralization stages (QTS and MOSS) constitute a continuous sequence, which was then superimposed and/or cross-cut by the latest mineralization stages (MSS, PAS and LCS).

The (QTS) corresponds to an early precursor of the W-Sn mineralization (MOSS) and marks the incipience of the hydrothermal activity in the mineralized veins of Panasqueira (Codeço *et al.*, 2017; Launay *et al.*, 2018; Carocci *et al.*, 2018). This stage consists of an intense tourmalinization of the metasedimentary host rock and the opening of fibrous quartz-tourmaline veinlets (Fig. 3d). Tourmalines are commonly associated with muscovite, apatite, W-rich rutile (Carocci *et al.*, 2018) and, in some cases, with wolframite and cassiterite. The QTS is generally directly followed by the W-Sn mineralizing stage (MOSS).

The MOSS carries the W-Sn mineralization and constitutes the most volumetrically important stage (≈ 60% of the vein volume) (Kelly and Rye, 1979; Polya *et al.*, 2000). The MOSS can be subdivided in two sub-stages:

(i) An early event marked by the crystallization of quartz-muscovite-apatite rich selvages along the schist vein contacts (Figs. 3e and 3f). This sub-stage is usually in direct continuity with tourmaline of the QTS. Cassiterite can be found within these selvages as intergrown with tourmaline and muscovite.

(ii) The sequence continued with a typical syntaxial overgrowth of the vein selvages marked by the crystallization of large euhedral crystals of quartz (Fig. 3f). This quartz crystallized preferentially vertically and perpendicularly to the schist-vein contact. During this sub-stage the veins exhibit geodic texture characterized by the presence

of large void spaces between the crystals of quartz (Fig. 3f). The crystallization of quartz was followed by the cavity-filling with muscovite, apatite, wolframite, and cassiterite. The wolframite occurs as large nugget-like aggregates that explain the extreme heterogeneous spatial distribution of wolframite in veins.

According to fluid inclusions studies (Kelly and Rye, 1979; Bussink, 1984) and boron isotope exchange between muscovite and tourmaline (Codeço *et al.*, 2019a), fluids involved during the QTS and the MOSS are characterized by temperatures ranging between 300–490 °C and moderate salinites (5–10 wt% NaCl eq.).

3 Methods

3.1 Sampling

Quartz and muscovite are ubiquitous in the earliest mineralization stages of veins, in the two-mica granite and in the greisen. These minerals constitute important witness to constrain hydrothermal processes involved during the greisenization and the W-Sn mineralization of Panasqueira. To study petrological and geochemical characteristics of quartz and muscovite of the granite intrusion and greisen, samples were collected in the drill hole SCB2 and within the cupola (Level 1 in mine). Samples of veins representative of the first mineralization stages (QTS and MOSS) were also collected. Samples with rich-apatite selvage were also collected to constrain the timing between the granite cooling, greisenization and the W-Sn mineralization stage by U-Pb dating of apatite. The locations of samples collected for this study are displayed in Figure 1.

3.2 Whole rock geochemistry

The whole rock major and trace element compositions of the selected samples of granite and greisen were determined following the analytical procedure of ALS laboratories. Samples were first crushed and pulverized and the finer faction was recovered (75 μm) for analyses. From these powders, the major element composition of samples was determined by inductively coupled plasma atomic emission spectroscopy (ICP-AES). For trace element analyses, a lithium borate fusion of each sample powder was performed. The melt produced by this method was then completely dissolved by acid digestion and trace element analyses were carried out by inductively coupled plasma mass spectrometry (ICP-MS).

3.3 Scanning electron microscopy (SEM) and cathodoluminescence imaging (CL)

Mineralogical and micro-textural characteristics of samples were examined on polished thin sections by optical microscopy (reflected and transmitted light) and by SEM using a Merlin compact Zeiss high resolution scanning electronic microscope equipped with a Gemini I detector (BRGM, University of Orléans). To display chemical zoning present in some minerals (like muscovite and apatite), element mapping was performed by SEM using an acceleration voltage of 15 kV.

The cathodoluminescence (Cl) images of quartz and apatite were collected at the BRGM (French Geological Survey) using a TESCAN MIRA 3 Scanning Electronic Microscope (SEM) equipped with a single channel panchromatic detector. This detector has a spectral range from 350 to 650 nm providing greyscale images of the Cl emissivity. Polished thick and thin sections were examined for a working distance of 16 mm with an accelerating voltage of 20 kV and a current of 15 nA. For the textural analysis of quartz, the image acquisition has been performed with a scanning speed ranging from 100 to 500 μs/pixel depending on the presence of highly luminescent minerals (apatite, carbonate) associated with quartz.

3.4 Electron microprobe analyses (EPMA)

The major and minor elements compositions of muscovite were determined on polished thin sections using a Cameca SX-Five electron probe micro-analyzers (EPMA) at the Institut des Sciences de la Terre d'Orléans (ISTO). Analyses were performed using an accelerating voltage of 15 kV, an electron beam current of 6 nA and a beam diameter of 2 μm. Elemental mapping of muscovite have been performed using an accelerating voltage of 20 kv. For calculation of structural formulae, the analyses were normalized to the total number of oxygens in the muscovite. Analytical conditions and calibration used for EPMA analysis of muscovite are detailed in the supplementary materials (ESM1A).

3.5 Laser ablation inductively coupled plasma mass spectrometry (LA-ICP-MS)

3.5.1 Trace elements analyses of muscovite

Concentrations of Si, Li, Zn, Rb, Sr, Nb, Sn, Cs, Ba, Ta and W in muscovite from granite, greisen and veins were determined on thin sections by LA-ICP-MS. These analyses were performed at the Laboratoire Géoscience Océan of Brest using a Thermo Element 2 ICP-MS coupled with a Compex Pro 102 Coherent 193 nm laser ablation system. Ablations were performed with a laser shot frequency of 5 Hz and beam size of 50 and 75 μm. Analyses comprise 20 s of gas blank measurement following by 60 s of ablation. The gas used to carry the ablated material to the ICP-MS was a He and Ar mixture. Concentrations were obtained with the Glitter 4.0 software (http://www.glittergemoc.com/) using the NIST SRM-612 (Pearce *et al.*, 1997) glass standard for external standardization, while BCR2 and BIR1 were used as supplementary control standards. Then, analyses of muscovite were normalized to ^{29}Si using concentrations obtained by EPMA. Analytical conditions and calibration used for trace element analysis of muscovite are detailed in the supplementary materials (ESM1B).

3.5.2 Trace elements analyses of quartz

The content of Li, Be, B, Na, Al, Si, S, Ti, Ge, As, Rb, Sr, Nb, Sn, Sb, Ta and W in quartz were determined by LA-ICP-MS. These analyses were performed at BRGM (French Geological Survey) using a ThermoScientific X series II quadrupole ICP-MS coupled with a Cetac Excite 193 nm laser

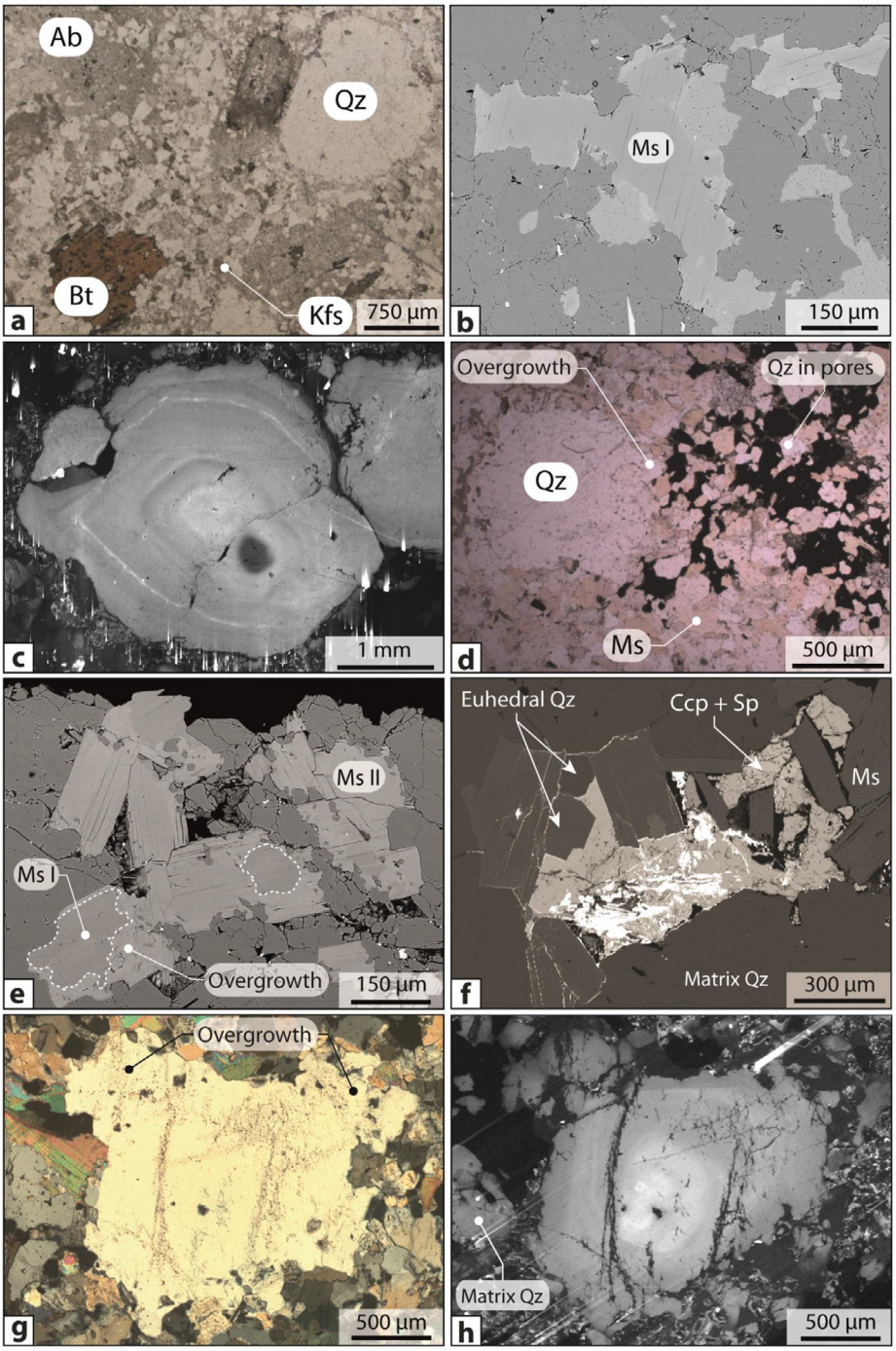

Fig. 4. Photomicrographs, SEM-BSE and SEM-CL images showing the textural characteristics of muscovite and quartz composing the two-mica granite and greisen of Panasqueira. (a) General view displaying the mineralogical composition and the texture of the two-mica granite. (b) SEM-BSE image of larges flakes of magmatic muscovite displaying unzoned microtexture. (c) SEM-CL image of euhedral magmatic quartz phenocryst composing the two-mica granite of Panasqueira. This quartz exhibits snowball texture with relatively weakly contrasted concentric growth zoning. (d) General view displaying the mineralogical composition and the texture of greisen. Note that vugs developed during greisenization were infilled by euhedral hydrothermal quartz and late sulphides and carbonate assemblages. (e) SEM-BSE image of muscovite composing the greisen of Panasqueira. These muscovites exhibit a strong zoning corresponding to hydrothermal overgrowth of primary magmatic muscovite of the two-mica granite. (f) SEM-BSE image of euhedral hydrothermal quartz infilling vug of greisen. Transmitted light (f) and SEM-CL (g) images of remnants of primary magmatic snowball-textured quartz partially altered during greisenisation. These quartz exhibit hydrothermal overgrowths characterized by lower luminescence intensity than primary snowball cores. In some cases the primary concentric growth zoning are conserved. The CL-dark structures correspond to healed fractures underlined by fluid inclusions trails in transmitted light. Ab: Albite, Bt: Biotite, Kfs: K-feldspar, Ms: Muscovite, Qz: Quartz.

ablation system. Ablations were performed on thick sections with a repetition rate of 8Hz and laser energy of 10 J/cm^2 with a beam size of 85 μm. The ablated material was transported from the laser ablation cell by a He gas with a flow rate of 250 mL/min. Analyses comprise 20 s of gas blank measurement following by 60 s of ablation. Data reduction was performed with the software Glitter 4.0 using the NIST SRM-612 glass standard for external standardization and the ^{29}Si isotope as internal standard assuming a SiO_2 content of 99 wt% in quartz. The relative standard deviation (RSD) between the measured and reference concentrations of the certified standard NIST-612 SRM are below 10% for all elements. Analytical conditions and calibration used for trace elements analysis of quartz are provided in the supplementary materials (ESM1C).

3.6 Statistical treatment approaches

To investigate the signature of muscovite and quartz composing the magmatic-hydrothermal system of Panasqueira, 5 populations of muscovite and 9 populations of quartz were distinguished based on their geological (magmatic, hydrothermal related to greisenization and hydrothermal related to mineralized veins) and petrographic characteristics. We performed two types of multivariate statistical analyses: (i) principal component analysis (PCA) and (ii) permutational multivariate analysis of variance (PERMANOVA; Anderson, 2001), which allows constraining the statistical similarities in element concentrations between the different populations. These statistical analyses were performed with Past 3.17 (Hammer *et al.*, 2001) following the procedure described by Monnier *et al.* (2018). In order to avoid of left-censored data, elements characterized by concentrations close or below to the (bdl) were not included for these statistical analyses.

3.6.1 Principal component analysis (PCA)

Principal component analysis (PCA) is a multivariate statistical method that permits to (i) reduce a large dataset into only two variables for plotting and clustering purposes and (ii) identify correlations between variables. This approach uses an orthogonal transformation to convert variables into a set of principal components (PC), which correspond to linear combinations of the initial variables. The first principal component (PC1) retains the maximum variance present in the original dataset. In geosciences this method is powerful tool to constrain the compositional variations of minerals between the differents populations (quartz and muscovite) and to investigate the behaviour of elements during geological processes (Winderbaum *et al.*, 2012; Belissont *et al.*, 2014; Monnier *et al.*, 2018). Here, we applied ACP to investigate geochemical patterns in whole rock, quartz and muscovite.

3.6.2 Permutational multivariate analysis of variance (PERMANOVA)

Permutation multivariate analysis of variance (PERMANOVA) is used to compare and quantify the degree of similarity between different populations considering here the element concentrations. A F-ratio is calculated between each populations by inter-point geometric approach that corresponds to scalar correlations based on the distance measure between any two objects (Anderson, 2001). This F-ratio permits to quantify the degree of similarity between populations. For values between −1 and 1 the two populations can be considered statistically identical and indistinguishable, while for high F values the two populations are statistically dissimilar. The calculation of F values was performed with Curtis-Bray distance measurement method with test of variables significance considering 9999 permutations (Anderson, 2001; Monnier *et al.*, 2018). Here, this quantification of the degree of similarity between the different populations of quartz and muscovite will allow determining potential genetic link between greisenization and the mineralized veins of Panasqueira.

3.7 U-Pb dating of apatite

U-Pb dating of apatite (magmatic and hydrothermal) was conducted by in-situ LA-ICP-MS analyses at Geosciences Rennes using a quadripole Agilent 7700x ICP-MS coupled to ESI NWR193UC excimer laser. Apatite was ablated with a constant spot diameter of 50 μm for an ablation rate of 5 Hz. The ablated material was then carried to ICP-MS by He mixed with N_2 and Ar. Analyses were performed according to the analytical procedure described by Pochon *et al.* (2016) and detailed in appendix (ESM1D). Analyses of apatite were bracketed by analyses of different apatite standards comprising (i) the Madagascar apatite standard (ID-TIMS age of 473.5 ± 0.7 Ma; Cochrane *et al.*, 2014) used as the primary apatite reference and (ii) the Durango (31.4 ± 0.12 Ma; McDowell *et al.*, 2005) and the McClure (523.5 ± 2.1 Ma; Schoene and Bowring 2006) apatite standards used to control the reproducibility and accuracy of measurements. Data reduction was performed following the procedure described by Pochon *et al.* (2016) using VizualAgeUcomPbine (Petrus and Kamber, 2012) and ages were calculated from the ISOPLOT software (Ludwig, 2012) that provides ages with 2σ error.

4 Microtextural charcateristics of quartz and muscovite

4.1 Two-mica granite

The mineralogical and the textural characteristics of the two-mica granite of Panasqueira are displayed in Figure 4a. As described previously, this granite exhibits a porphyritic, coarse grained texture (Fig. 4a).

Muscovite forms individual large sub-euhedral flakes (up to 1–2 mm) (Fig. 4b) consistent with a primary magmatic origin according to the textural criteria given by Miller *et al.* (1981). They occur as interstitial grains in the rock matrix and as micaceous aggregates. Although the main part of muscovite appears to be igneous origin, some little flakes of muscovite can be observed along grain boundaries of biotite and feldspars and could result from hydrothermal alteration of these minerals. Backscattered electron images show that muscovite is characterized by a homogeneous chemical composition (Fig. 4b).

Quartz occurs as large euhedral grains (up to 0.5 cm) characterized by snowball texture (Figs. 4a and 4c). This

texture is particularly common in highly evolved granitic systems related to rare-metal mineralization (Sn-W-Nb-Ta) (Charoy and Noronha, 1991; Müller and Seltmann, 1999; Müller *et al.*, 2002, 2018). These snowball-textured quartz are characterized by straight and sharp boundaries (Fig. 4c) and can contain small inclusions of albite and muscovite. The extinction of this quartz is homogeneous suggesting the absence of plastic deformation in quartz. However, the presence of fluid inclusions trails attests that snowball quartz were affected by fracturing and healing mechanism that probably occurred after the granite cooling (Fig. 4c). As evidenced by cathodoluminescence images (CL), snowball quartz exhibits weakly contrasted, oscillatory growth zoning (Fig. 4c). Cores are generally marked by higher luminescence intensity than rims. Fluid inclusions trails observed in transmitted light correspond to Cl-dark structures defining healed vein-like structures that result from the precipitation of non-luminescent quartz within fractures planes (Rusk and Reed, 2002). Quartz occurs also as small xenomorph grains in the granite matrix (Fig. 4a). This second population of quartz is usually characterized by low CL and displays the same luminescence intensity than rims of snowball quartz.

4.2 Quartz-muscovite greisen

Mineralogical and textural characteristics of the quartz-muscovite greisen are displayed in Figure 4d. As evidenced from petrographic observations, greisenization of the two-mica granite has caused the total breakdown of biotite and feldspars, which were replaced by a large amount of muscovite and quartz. During this intense metasomatic alteration the primary magmatic texture was completely obliterated. However, relics of snowball-textured quartz and primary magmatic muscovite can be observed in greisen (Fig. 4d).

Muscovite composing the massive greisen forms large subeuhedral flakes (Figs. 4e and 4f). Some of them are characterized by a well-developed growth zoning marked by dark cores and light rims in SEM-BSE images (Fig. 4e). The contact between core and rim is well defined and the thickness of rims ranges between 50 and 300 μm. Such pattern was already described in ongonites (Dostal *et al.*, 2015) and in the hydrothermally altered Sn-bearing granite of Ervedosa (northern Portugal) (Gomes and Neiva, 2000). It is usually interpreted as marker of the hydrothermal alteration related to mineralization event. Accordingly, these zoning can be interpreted as hydrothermal overgrowths of the primary magmatic muscovite during greisenization. Hydrothermal muscovite that have exclusively crystallized during greisenization (MsII) exhibit homogeneous light color and are generally unzoned (Fig. 4e).

Remnants of primary magmatic snowball quartz that were partially altered during the greisenization can be observed in greisen (Figs. 4d and 4g). They are generally characterized by irregular shape marked by the presence of hydrothermal overgrowths likely formed during greisenization (Figs. 4g and 4h). Inclusions of albite and muscovite can be observed in these hydrothermal overgrowths (Fig. 4g). In cathodoluminescence images, these grains exhibit irregularly shape CL-light cores (primary magmatic snowball-textured quartz) surrounded by very weak luminescent quartz (hydrothermal overgrowth) (Fig. 4h). Quartz composing the greisen matrix and formed during greisenization by feldspars and biotite replacement is xenomorph and characterized by low luminescence intensity (Fig. 4h). The euhedral quartz observed in the greisen porosity in association with cassiterite and sulphides (Figs. 4d and 4f) is marked by very weak CL equivalent to those observed in the matrix quartz. Secondary structures as healed fractures are common in all quartz composing the massive greisen.

4.3 Ore-bearing quartz veins

The textural characteristics of the muscovite selvage present along the schist-vein contacts and quartz related to the QTS and MOSS are displayed in Figure 5. Muscovite selvages exhibit a fibrous texture composed of large euhedral flakes (that can reach 3 cm of height) that grew vertically during the opening of veins (Fig. 5a). Muscovite is generally found in direct continuity with tourmaline formed during the quartz tourmaline stage (QTS) and can be associated with apatite, cassiterite and wolframite (Fig. 5a). This muscovite is generally unzoned but brighter-luminescent overgrowth can be locally observed.

Quartz of the hydrothermal veins forms generally prismatic megacryst that can reach ~20 cm of length. In general, quartz grew vertically and perpendicular to the vein edge. On sections perpendicular to their axis, quartz exhibit typical euhedral shape surrounded by large cavities, in which cassiterite and wolframite have then crystallized (Figs. 5b and 5c). Tourmaline is generally anterior and included within these crystals of quartz (Fig. 5b). As evidenced by CL images this quartz is characterized by thin, contrasted, oscillatory growth zoning (Figs. 5d and 5e). Sector zoning emphasizes implication of corrosion processes during which quartz could be partially dissolved and re-crystallized (Fig. 5e). Hydrothermal quartz is also distinguished by a dense network of secondary structures composed of fractures healed by non-luminescent quartz (Figs. 5d and 5e).

5 Whole-rock geochemistry

Bulk analyses of the two-mica granite, greisenized granite and massive greisen of Panasqueira are provided in supplementary materials (ESM2). The Panasqueira two-mica granite belongs to rich-phosphorous granites (0.35 to 0.44 wt%) and exhibits peraluminous compositions, with alumina saturation index A/CNK (molar $Al_2O_3/CaO + Na_2O + K_2O$) ranging from 1.17 to 1.39 and agpaitic index A/NK (molar $Al_2O_3/Na_2O + K_2O$) between 1.28 and 1.46 (Fig. 6a and ESM2). In the Nb/Ta *vs.* Zr/Hf diagram (Ballouard *et al.*, 2016) the compositions of the Panasqueira two-micas granite fall in the field of granites related to Sn-W mineralization (Fig. 6b). The greisenization of this two-mica granite is accompanied by an evolution trend marked by progressive increase of the aluminium content with A/CNK rising to 2.39 and A/NK up to 2.73 (Fig. 6a).

Results of PCA performed on all whole-rock elemental compositions of the two-mica granite, greisenized granite and greisen are displayed in Figure 6c. A set of 21 variables has

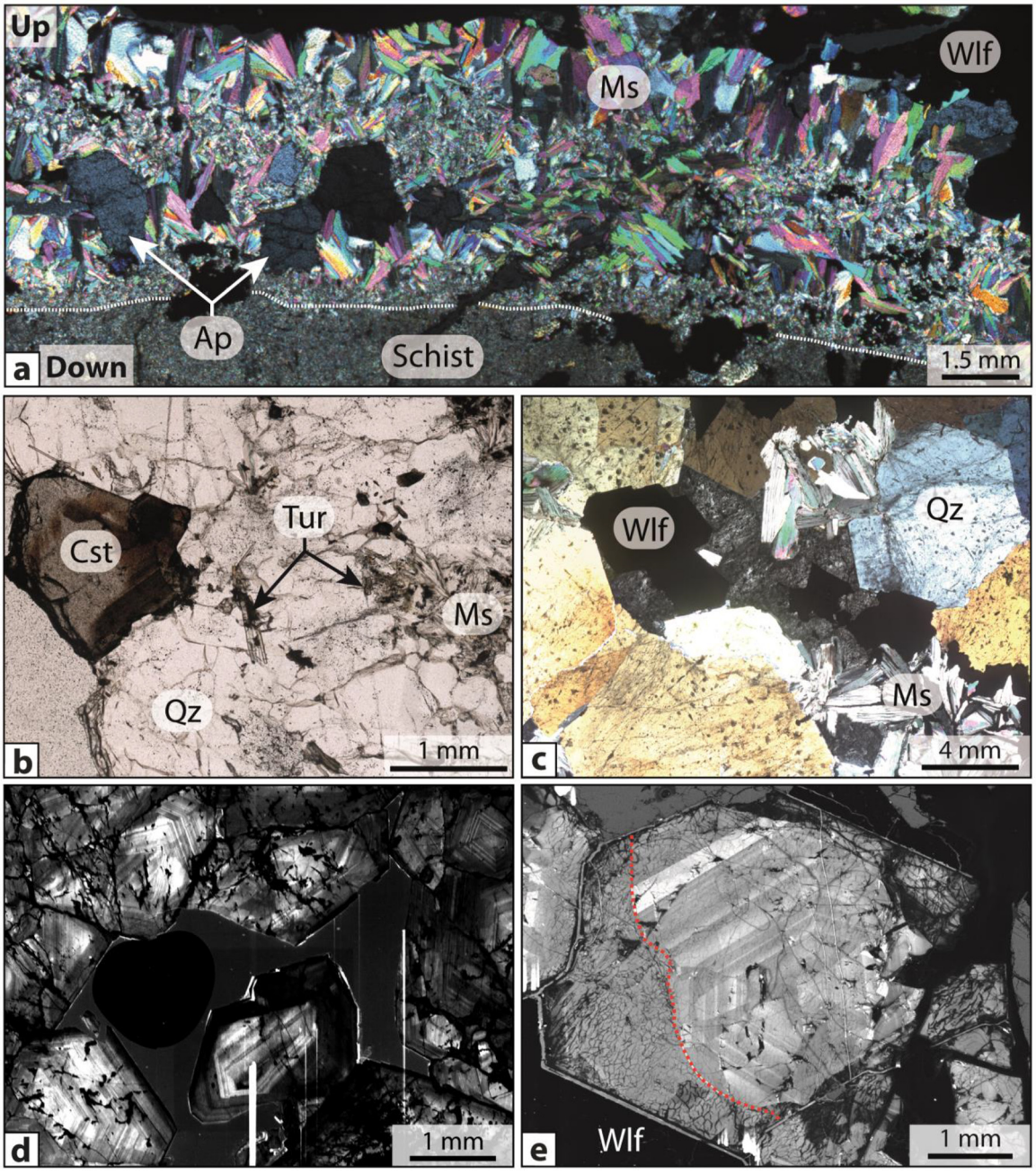

Fig. 5. Photomicrographs and SEM-CL images showing the textural characteristics of muscovite and quartz related to the QTS and MOSS of the mineralized veins of Panasqueira. (a) Vertical section perpendicular to the horizontal vein planes showing a muscovite-rich selvage associated with early apatite and overlain by wolframite. (b) and (c) transmitted light images of hydrothermal quartz respectively formed during to the QTS and the MOSS. These sections were cut horizontally and perpendicular to the axis of quartz. (d) and (e) SEM-CL images displaying textural characteristics of quartz formed during the QTS and the MOSS. These hydrothermal quartz exhibit thin, contrasted, oscillatory growth zoning. The dense network of CL-dark structures corresponds to fractures healed by non-luminescent quartz. Quartz can be partially corroded (red dashed line in e) and marked by sector zoning. Ap: Apatite, Cst: Cassiterite, Ms: Muscovite, Qz: Quartz, Tur: Tourmaline, Wlf: Wolframite.

been selected for this PCA including major elements (Fe, Mg, Ti, Ca, Na, K, Mn and P), the main trace elements (Li, Ba, Cs, Nb, Ta, Rb, Sr, W, Sn, Zn, Cu and ΣREE) and the A/CNK ratio, which as mentionned above is positively correlated with the degree of greisenization of samples. The PC1 *vs.* PC2 projection plane (Fig. 6c) accounts for 69.1% of the total variance of the dataset, with 51.3% for PC1 and 17.8% for PC2. Samples of two-mica granite (black dots on the left side of Fig. 6c) are separated of greisen samples (white dots on the right side of Fig. 6c) by PC1, which is strongly loaded by metal-granophile elements (Cs, Rb, Nb, Ta, Sn, W, Cu and Zn) and the A/CNK ratio. Greisenized granite samples (grey dots) occupy an intermediate position between granite and greisen samples that is consistent with evolution trend observed in

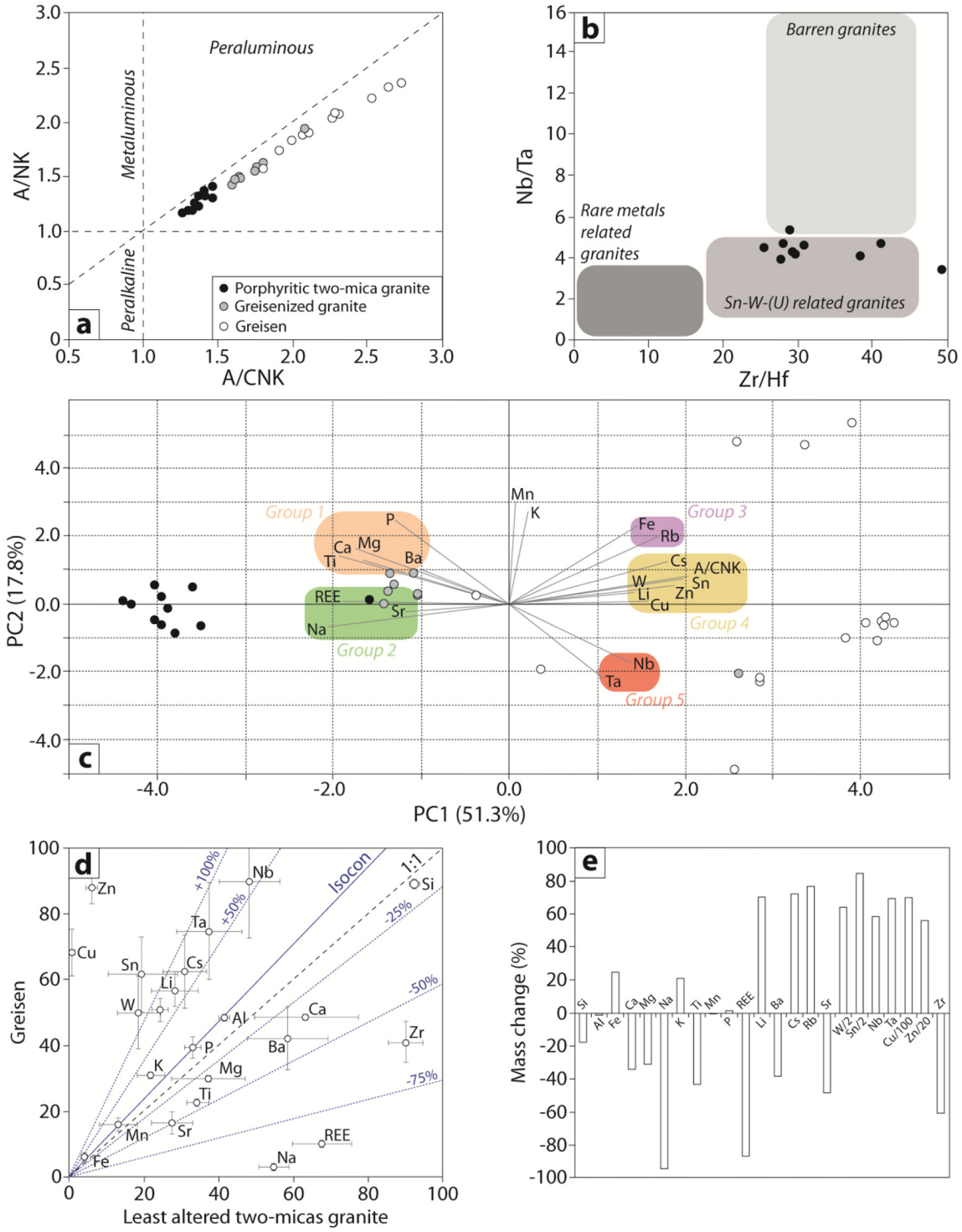

Fig. 6. Whole-rock geochemical characteristics of the two-mica granite and the massive greisen of Panasqueira. (a) Diagram of aluminous saturation index (A/NK *vs.* A/CNK). (b) Nb/Ta *versus* Zr/Hf diagram discriminating barren to ore-bearing peraluminous granites (modified from Ballouard *et al.*, 2016). (c) Biplot PC1 *vs.* PC2 diagram displaying results of principal components analysis (PCA) performed on major and trace element compositions of granite, greisenized granite and greisen. (d) Isocon diagram displaying the mobility of elements during greisenization. The lines with percentage values correspond to the net percent gains and losses relative to the isocon (blue line). Granite and greisen compositions are respectively an average of the 11 least altered granite and the 3 most altered samples of greisen. (e) Major and trace elements mass changes in greisen relative to the best fit isocon.

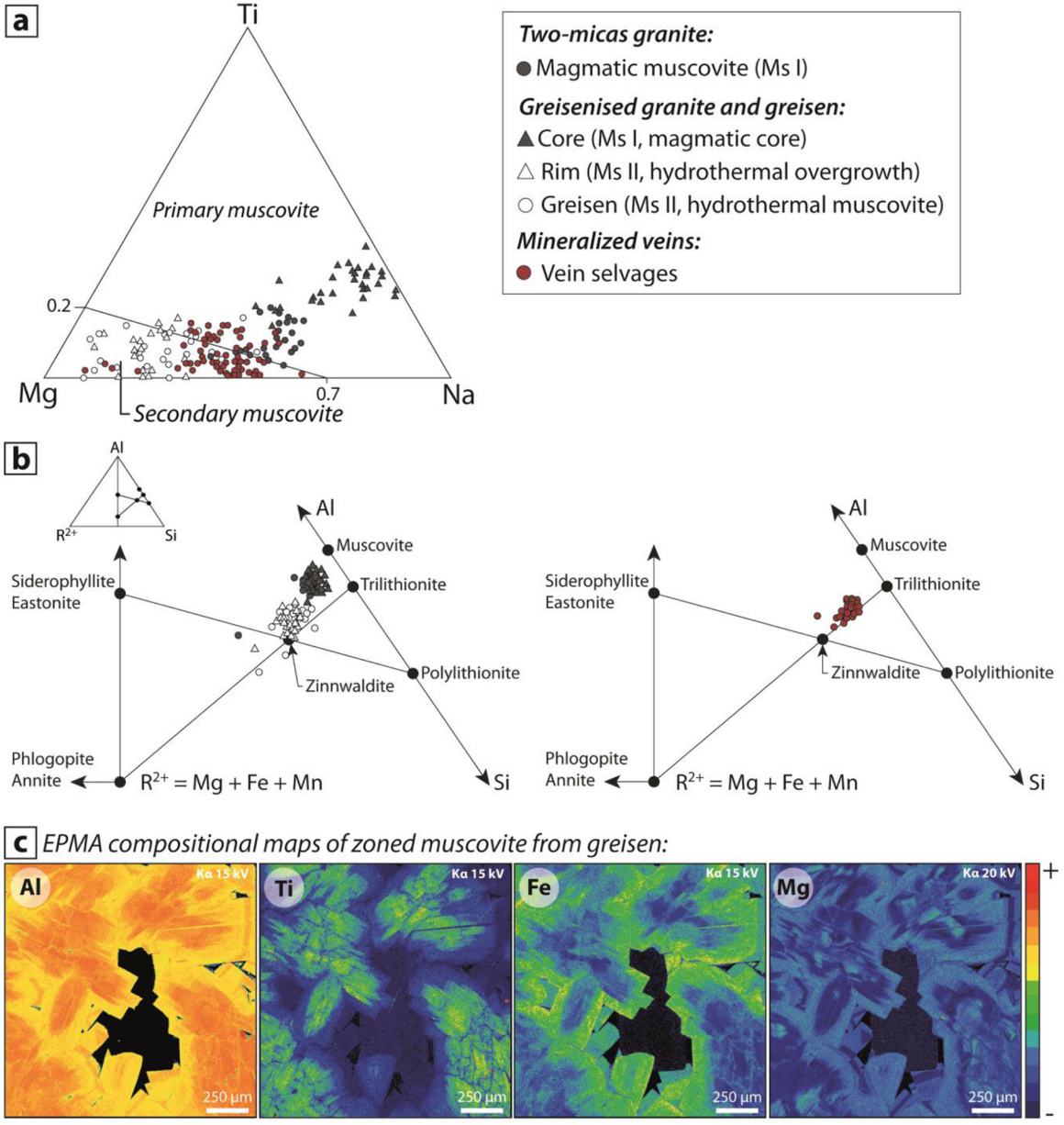

Fig. 7. Geochemical characteristics of muscovite composing the two-mica granite, greisenized facies, the massive greisen and the mineralized veins selvages of Panasqueira. (a) Ternary Ti-Na-Mg diagram displaying the fields of primary and secondary muscovite (after Miller *et al.*, 1981). (b) Compositions of muscovite plotted in the mineralochemical phase diagrams (Al-(Fe + Mg + Mn)-Si) of Monier and Robert (1986). (c) Chemical maps of Al, Ti, Fe and Mg of muscovites composing the greisen of Panasqueira. These muscovites exhibit a strong chemical zoning corresponding to hydrothermal overgrowths of primary magmatic muscovites.

Figure 6a. Five element clusters in which elemental concentrations are positively correlated can be distinguished (Fig. 6c): the group 1 (Mg, Ti, Ba, Ca and P), the group 2 (Na, Sr and ΣREE), the group 3 (Fe and Rb), the group 4 (Sn, W, Li, Cs, Cu, Zn and A/CNK) and the group 5 (Nb and Ta). Elements composing the group 3, 4 and 5 are anti-correlated with elements composing the group 1 and 2 (Fig. 6c). Granite is generally rich in elements composing the groups 1 and 2 whereas greisen is enriched in elements composing groups 3, 4 and 5.

In order to constrain mass changes (*i.e.* element gains and losses) and element mobility related to greisenization, mass balance was performed using the Grant's (Grant, 1986) isocon approach (Fig. 6d). The best fit isocon (blue line in Fig. 6d) is drawn using Al, Mn and P, assuming that these elements were conservative and relatively immobile during greisenization. The slope of this isocon (~1.18) suggests an important mass loss during greisenization that is consistent with the abundant porosity observed in greisen (Launay, 2019). Individual element mass changes calculated from the isocon are displayed

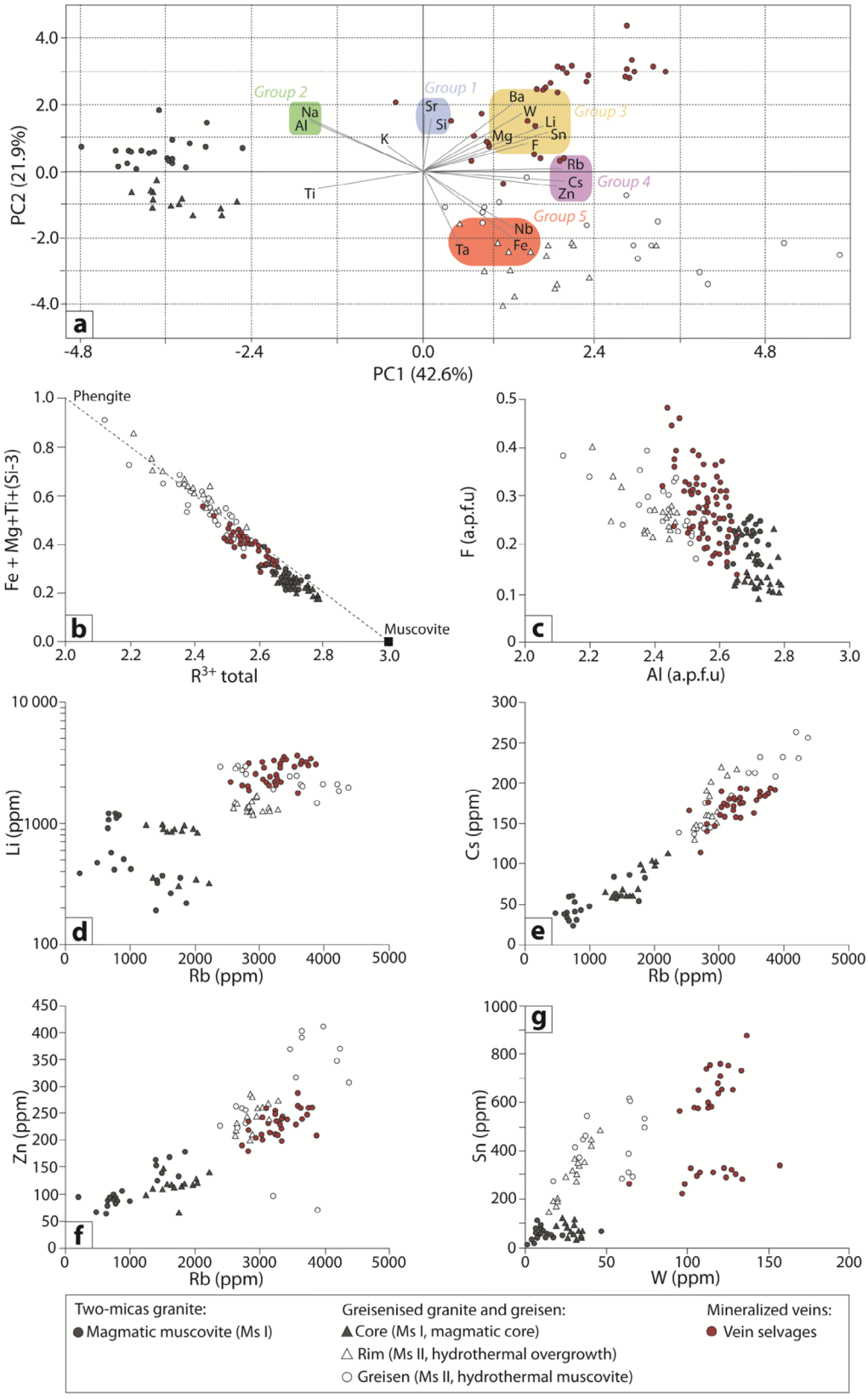

Fig. 8. (a) Biplot PC1 *vs.* PC2 diagram displaying results of principal components analysis (PCA) performed on major and trace element compositions of the different generations of micas composing the two-mica granite, the greisenized facies, the greisen and the mineralized vein selvages of Panasqueira. (b) Diagram illustrating ideal dioctahedral substitutions for different populations of micas (after Guidotti, 1984). (c) to (g) Binary diagrams displaying the major and trace element content for the different generations of muscovite considered in this study. The elements pairs displayed in these diagrams were defined from PCA performed on the muscovite composition dataset.

Table 1. F-values obtained by PERMANOVA for the different populations of muscovite composing the two-mica granite, the greisenized granite facies, the massive greisen and the mineralized veins selvages of Panasqueira. Lowest F-values are highlighted in red to display principal similarities between the different pairs of muscovite generations.

	Two-mica granite		Greisenised granite and greisen		Mineralized veins
	Magmatic muscovite	Magmatic core	Hydrothermal overgrowth	Hydrothermal muscovite	Vein selvages
Magmatic muscovite		-	-	-	-
Magmatic core	**9.45**		-	-	-
Hydrothermal overgrowth	63.77	93.71		-	-
Hydrothermal muscovite	83.23	136.7	**13.09**		-
Vein selvages	129.6	153	**18.96**	32.41	

in diagram of relative mass changes (Fig. 6e). Greisen is marked by an overall enrichment in Fe (24%), K (20.5%), Cs (72%), Rb (77%), Li (70%), Sn (170%), W (129%), Nb (58%), Ta (69%), Cu (7000%) and Zn (1120%) and depletion in Si (−18%), Mg (−32%), Ca (−35%), Na (−95%), Ti (−44%), Ba (−39%), Sr (−49%), Zr (−61%) and REE (−87%). This evolution is consistent with element clusters identified by PCA and reflect the mineralogical control on the incorporation and releasing of elements during fluid-rock interactions related to the greisenization. Indeed, the breakdown of K-feldspar and albite have released Ba, Na and Sr (group 1 and 2 in Fig. 6c), while the destruction of biotite has released Mg and Ti into fluids (group 1 in Fig. 6c). Conversely, the crystallization of a large amount of muscovite was likely responsible of the enrichment in Li, Cs and Rb (group 4 and 5) observed in greisen. The depletion of greisen in REE can be attributed to the breakdown of accessory minerals hosting REE (like zircon and monazite) (Stemprok *et al.*, 2005; Müller *et al.*, 2018). The enrichment of greisen in Nb, Ta, Sn, W, Cu and Zn (elements of group 4 and 5 in Fig. 6c) is likely related to the circulation of ore-bearing fluids through the granite's roof.

6 Muscovite geochemistry

Major and trace elements compositions of muscovite composing the two-mica granite, the greisenized granite, the massive greisen and the mineralized veins of Panasqueira are provided in supplementary materials ESM3 and ESM4.

6.1 General features and classification

All white-micas described previously are classified according to the discriminating diagrams of Miller *et al.* (1981) and Monier and Robert (1986) (Figs. 7a and 7b). White-mica composing the two-mica granite falls in the primary muscovite field (Fig. 7a) and is characterized by compositions close to theoretical muscovite according to the classification of Monier and Robert (1986) (Fig. 7b). Hydrothermal muscovite formed during the greisenization and composing the massive greisen fall in the secondary muscovite field (Fig. 7a) and are characterized by compositions ranging from muscovite to Zinnwaldite (Fig. 7b). In chemical maps (Fig. 7c), the muscovite zoning texture corresponds to core to rim depletion in Al and Ti and core to rim enrichment in Fe and Mg. The cores of this muscovite fall in the primary muscovite field and are characterized by compositions close to the primary magmatic muscovite of the two-mica granite, while rims fall in the secondary muscovite field and exhibit almost the same compositions than secondary hydrothermal muscovite formed during the greisenization (Figs. 7a and 7b). Accordingly, the rims correspond likely to hydrothermal overgrowth of the primary magmatic muscovite. The overgrowths were formed during the greisenization and hence were likely equilibrated with greisenizing fluids. Hydrothermal white-mica composing the selvages along the schist-vein contacts are characterized by compositions ranging from trilithionite to zinnwaldite (Fig. 7b) and fall in part in the secondary muscovite field (Fig. 7a).

6.2 Major and trace elements compositional characteristics

Results of PCA performed on muscovite compositions are displayed in Figure 8a. PC1 and PC2 account respectively for 42.6% and 21.9% of the total variance of the dataset. The clustering of elements as well as the different populations of muscovite can be observed on the PC1 *vs.* PC2 projection plane (Fig. 8a). Indeed, magmatic muscovite (Ms I) composing the two-mica granite and the cores of muscovite occurring in the greisenized facies (left side of the diagram) are clearly separated of hydrothermal muscovite composing greisen (Ms II) and the vein selvages (right side of the diagram) by PC1.

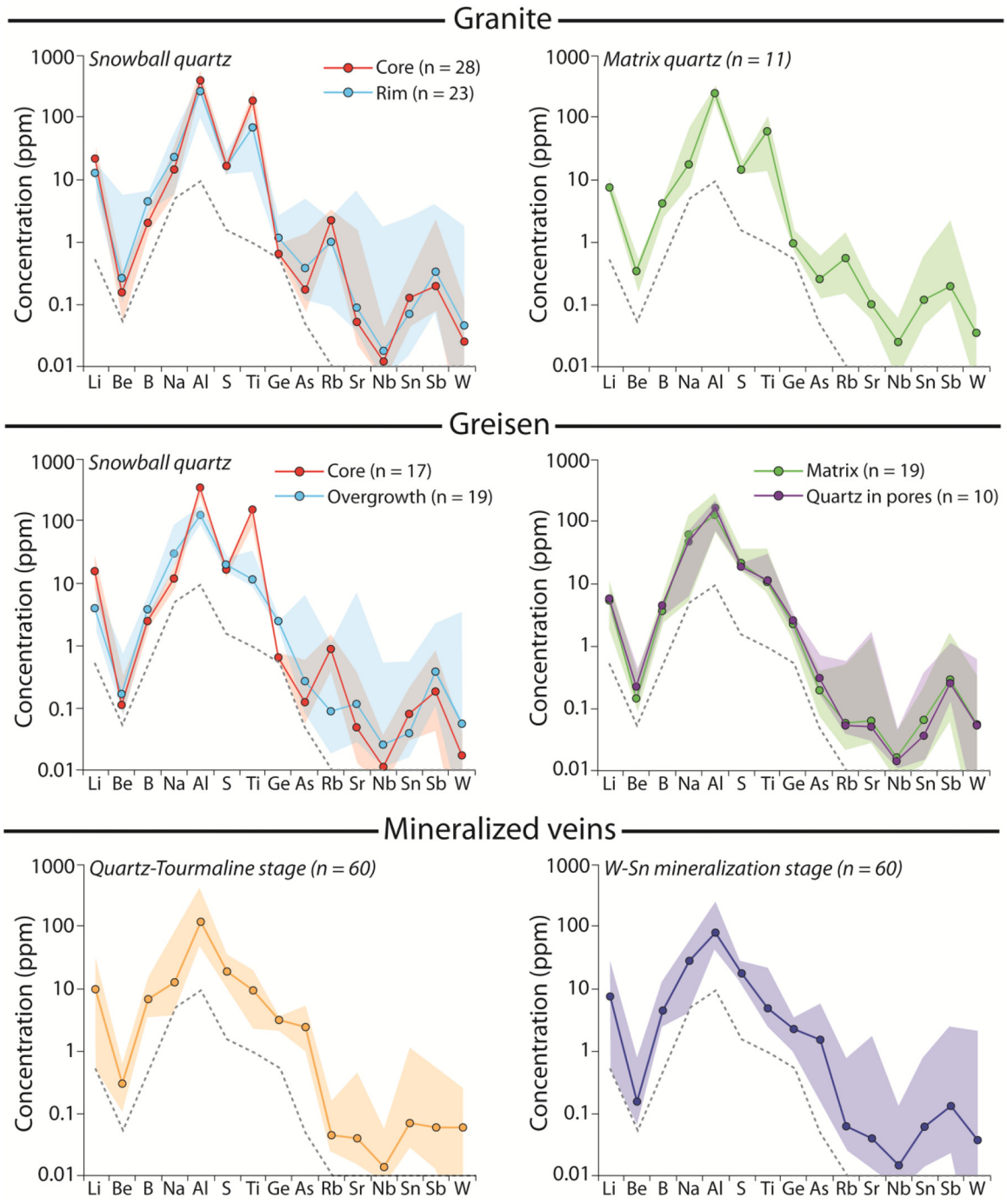

Fig. 9. Spider diagrams displaying trace element contents in the different generations of quartz considered in this study. The grey dashed line corresponds to the detection limit. Color lines correspond to median values for each quartz generation. Color domains were defined from maximal and minimal concentrations for each element.

The loading of PC1 is mainly influenced by Rb, Cs, Zn and to a lesser extent by F, Sn, W, Mg, Li and Ba. Muscovite compositions show positive correlations of elements and five element correlation clusters can be distinguished (Fig. 8a): the group 1 (Si and Sr), the group 2 (Na and Al), the group 3 (Ba, Mg, Sn, W, Li and F), the group 4 (Rb, Cs and Zn) and the group 5 (Fe, Nb and Ta). Elements composing the group 4 are positively correlated with elements composing the group 3 and 5 and anti-correlated with elements composing the group 2 (Fig. 8a). Elements composing group 3 and 4 are strongly anti-correlated with Ti.

As highlighted from binary diagrams (Figs. 8b–8g) and PC1-PC2 projection plane, the primary magmatic muscovites (Ms I) (from the two-mica granite and cores of zoned muscovite) are richer in Al, Ti and Na and poorer in Fe, Mg, F, Cs, Rb, Li, Zn, Sn and W than secondary hydrothermal

muscovite composing greisen (Ms II) (rims of zoned muscovite and muscovite formed by replacement of feldspars). The transition from Ti-rich magmatic muscovite to Ti-poor hydrothermal muscovite is consistent with chemical and thermic evolution of magmatic-hydrothermal system, during which muscovite composition was first controlled by hot magmatic processes and then by hydrothermal processes (Luhr *et al.*, 1984 Miller *et al.*, 1981; White *et al.*, 2007; Tartèse *et al.*, 2011). Figure 8b shows that the lower Al content in hydrothermal muscovite from greisen is balanced by the addition of Fe and Mg in the octahedral site by the substitution vector $(Mg, Fe)^{VI} \leftrightarrow Al$ explaining the higher Fe and Mg concentrations in muscovite composing greisen. The higher F content in hydrothermal muscovite composing greisen is consistent with fluid-rock interactions between granitic rocks and acidic F-rich magmatic fluids commonly observed and described in greisen systems (Shcherba, 1970; Stemprok, 1987; Bishop, 1989; Lehmann, 1990). The increase of the Rb content between magmatic muscovite from granite and hydrothermal muscovite of greisen is accompanied by significant increase of Cs, Li and Zn concentrations (Figs. 8d–8f). The Sn and W variations during greisenization are positively correlated and increase respectively from 60 to 414 ppm and 10 to 43 ppm (Fig. 8g). Hydrothermal muscovite from ore-bearing quartz veins exhibit intermediate compositions in Al, Mg, Fe and F between magmatic muscovite of granite and hydrothermal muscovite of greisen (Figs. 8b and 8c). They are also characterized by similar compositional ranges in Li, Ba, Cs, Rb and Zn and higher concentrations in W (between 65 and 156 ppm) and Sn (between 229 and 879 ppm) than hydrothermal muscovite composing the massive greisen.

6.3 Results of PERMANOVA

Results of PERMANOVA performed on the elemental compositions (Si, Ti, Al, Fe, Mg, Na, K, F, Li, Rb, Sr, Nb, Sn, Cs, Ba, Ta and W) of the different populations of muscovite are summarized in Table 1. As mentionned previously the similarity between two populations is strong when the F-value is low and weak when the F-value is high. For F-values between −1 and 1, the two populations can be considered undiscernable. Magmatic muscovites composing the two-mica granite (Ms I) are similar to cores of muscovite composing greisenized granite with an F-value of 9.45. Conversely, magmatic muscovites and hydrothermal muscovites composing the greisen and the mineralized veins selvages are strongly dissimilar with F-values exceeding 100 (Tab. 1). PERMANOVA shows also that rims of muscovite composing greisenized facies are similar to hydrothermal muscovite composing the greisen (Ms II) (F-value of 13.09) and the vein selvages (F-value of 18.96). These results confirm that cores of zoned muscovite composing the greisenized facies correspond to primary magmatic muscovite composing the two-mica granite. Moreover, similarities between the different populations of hydrothermal muscovite from greisen and mineralized veins suggest that these muscovite could crystallized from the same hydrothermal fluids.

7 Quartz chemistry

7.1 Chemical characteristics of the different generations of quartz

Li, Be, B, Na, Al, S, Ti, Ge, As, Rb, Sr, Nb, Sn, Sb, Ta and W were analyzed for the different quartz generations. Trace elements contents are reported as spider diagrams (Fig. 9) (the entire dataset is available in supplementary materials ESM5). Although the main part of analyzed elements was generally detected for all quartz generations, the concentrations in Be, Nb, Ta, Sn and W were often close to their detection limits (0.05 ppm for Be and 0.01 ppm for the other). Al, Li, Ti, Na and S are the most abundant elements (several tens to several hundred of ppm) in all quartz generations. Light elements like Ge and B were also significantly detected (up to several tens of ppm) in all quartz generations, whereas heavy elements contents (from As to W) are generally lower and characterized by wide ranges of concentrations (Fig. 9). Nb and Ta were generally not detected and hence are not considered to discriminate the different quartz generations. Al, Ti and Rb depict peaks specific of magmatic quartz, while Ge, B, As and W contents are generally higher in hydrothermal quartz composing both greisen and mineralized veins (Fig. 9).

Quartz from the unaltered two-mica granite: Cores of magmatic snowball-textured quartz are characterized by high contents in Ti (> 136 ppm), Al (> 295 ppm) and Li (> 10 ppm) and low content in B (< 3.4 ppm) and Ge (< 0.9 ppm). Snowball-textured quartz are generally marked by slight core to rim enrichments in Ge (from 0.6 to 1.1 ppm), B (from 2.1 to 4.2 ppm) and Na (from 14 to 22 ppm) and by slight core to rim depletion in Ti (from 183 to 64 ppm), Li (from 23 to 13 ppm), Al (from 408 to 263 ppm) and Rb (from 2.2 to 1 ppm) (values refer to median values for cores and rims). These rims exhibit also highly variable concentrations in Be, As, Rb, Sr, Nb, Sn, Sb and W. Quartz composing the granite matrix are characterized by the same median concentrations in trace elements than rims of snowball quartz. Accordingly, these two populations of quartz have probably crystallized sub-contemporaneously and later than cores of snowball quartz.

Quartz from the massive greisen: Snowball-textured quartz conserved in greisen exhibits the same spider diagram pattern and is characterized by the same compositional ranges than snowball quartz of the unaltered two-mica granite (Fig. 9). Indeed it displays the same typical peaks in Ti, Al and Rb previously described in magmatic quartz with almost the same median values of concentrations. This suggests that despite the strong fluid-rock interactions related to the greisenization, the primary magmatic signature of snowball-textured quartz was conserved in greisen, in which a large amount of secondary and recrystallized quartz were formed during the greisenization. Hydrothermal overgrowth of these snowball-textured quartz are characterized by a spider diagram pattern significantly different than magmatic snowball-textured quartz, with lower content in Ti (< 36 ppm), Al (< 140 ppm) and Rb (< 1.2 ppm) and higher content in Ge (> 1.8 ppm), B (> 3.1 ppm) and Na (> 20 ppm). Euhedral quartz from the greisen porosity exhibits the same signature than (i) neoformed quartz composing the greisen matrix and (ii) hydrothermal overgrowth of snowball

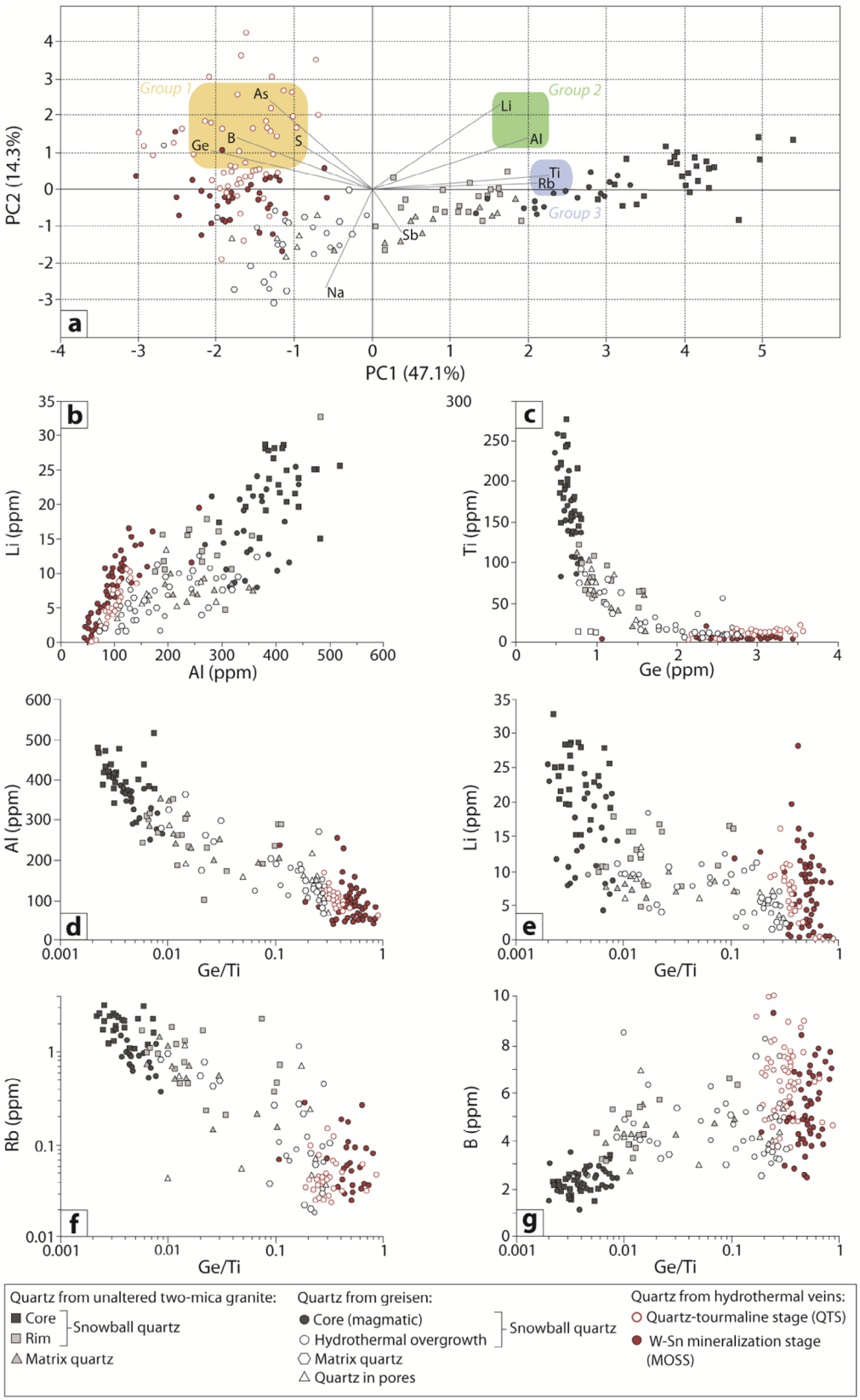

Fig. 10. (a) PC1 *vs.* PC2 projection plane displaying results of principal components analysis (PCA) performed on the main trace elements composing the different generations of quartz occurring in the two-mica granite, the greisen and the mineralized veins of Panasqueira. (b) to (g) Chemical evolution trends from magmatic to hydrothermal quartz displaying the behavior of Ti, Al, Ge, Li, Rb and B during magmatic-hydrothermal evolution of the Panasqueira ore deposit.

Table 2. F-values obtained by PERMANOVA for the different generations of quartz composing the two-mica granite, the greisen and the mineralized veins of Panasqueira. Lowest F-values are highlighted in red to display principal similarities between the different pairs of quartz generations. For F-values between −1 and 1 the populations are undiscernable.

		Two-mica granite			Greisenized granite and greisen				Mineralized veins	
		Core of snowball quartz	Rim of snowball quartz	Matrix quartz	Core of snowball quartz	Hydrothermal overgrowth	Matrix quartz	Quartz in pores	Quartz-Tourmaline stage (QTS)	W-Sn stage (MOSS)
Two-mica granite	Core of snowball quartz		-	-	-	-	-	-	-	-
	Rim of snowball Quartz	71.25		-	-	-	-	-	-	-
	Matrix quartz	75.3	**0.56**		-	-	-	-	-	-
Greisenized granite and greisen	Core of snowball quartz	**29.57**	**17.32**	**20.4**		-	-	-	-	-
	Hydrothermal overgrowth	336.9	40.75	39.77	180.2		-	-	-	-
	Matrix quartz	135.3	20.63	**14.78**	62.2	**2.13**		-	-	-
	Quartz in pores	176	19.7	18.11	90.27	**1.06**	**0.76**		-	-
Mineralized veins	Quartz-Tourmaline stage (QTS)	117.3	22.82	14.44	49.6	**4.57**	**4.76**	**2.49**		-
	W-Sn stage (MOSS)	393.4	106.4	74.77	206.5	14.14	21.09	**11.93**	29.53	

quartz (Fig. 12). Indeed, these different generations of quartz are marked by (i) the absence of peaks in Ti and Rb, (ii) highly variable concentrations in As, Rb, Sr, Nb, Sn, Sb and W and (iii) higher contents in B, Na and Ge compared to magmatic quartz. Accordingly, quartz crystallized during the greisenization by (i) feldspars and biotite replacement, (ii) overgrowth of snowball quartz and (iii) porosity infilling were formed and equilibrated with the same hydrothermal fluid in the same range of temperature as highlighted by Ti content, which is temperature-dependant.

Quartz from the mineralized veins: Hydrothermal quartz from mineralized veins related to the quartz-tourmaline (QTS) and the W-Sn mineralization stages exhibits signatures clearly different than those of magmatic quartz and close to signatures of hydrothermal quartz from greisen, with (i) absence of Ti and Rb peaks, (ii) lower contents in Al, Ti and Li and (iii) higher contents in Ge, B and Na than magmatic quartz. However, median As and B concentrations in hydrothermal quartz from veins (from 1.6 to 2.5 ppm for As and from 4.9 to 6.6 ppm for B) are significantly higher than those of hydrothermal quartz from greisen (from 0.08 to 0.29 ppm for As and from 3.8 to 4.2 ppm for B). Although quartz formed during the W-Sn mineralization stage has globally similar chemistry to quartz formed during the QTS, they are characterized by lower median concentrations in B, Al and Ti and higher median concentrations in Na than quartz of the QTS. Despite highly variable concentrations, W content in hydrothermal quartz from veins (up to 5.8 ppm) and greisen (up to 3.5 ppm) seem to be higher than in magmatic quartz (up to 1.7 ppm).

7.2 Chemical evolution trends

Results of PCA performed on the trace element compositions of quartz are shown in Figure 10a. The clustering of quartz populations is clear on PC1-PC2 projection plane. Magmatic quartz occurs on the right side of the diagram and is clearly separated of hydrothermal quartz that occurs on the left side (Fig. 10a). Higher concentrations in Ge, B, As and S (group 1) and lower concentrations in Li, Al, Ti and Rb (group 2 and 3) distinguish hydrothermal quartz (from greisen and mineralized veins) from magmatic quartz. As expected from PCA, Li and Al (group 2) show positive linear correlation (Fig. 10b) for both magmatic quartz and the different generations of hydrothermal quartz. This correlation commonly described in magmatic-hydrothermal systems (Breiter *et al.*, 2017; Müller *et al.*, 2018; Monnier *et al.*, 2018) is due to the coupled substitution $Al^{3+} - Li^{+} \leftrightarrow Si^{4+}$ (Weil, 1984; Heaney *et al.*, 1994; Götze *et al.*, 2004). The chemical trend depicted in the Li *vs.* Al diagram exhibit a progressive depletion in Al and Li from magmatic quartz of the two-mica granite to hydrothermal quartz of greisen and mineralized veins (Fig. 10b). The Ge and Ti are strongly anti-correlated (Figs. 10a and 10c). Indeed, the Ge *vs.* Ti diagram (Fig. 10c) displays a progressive Ti depletion and progressive Ge enrichment from magmatic quartz to hydrothermal quartz of greisen and mineralized veins. This negative correlation is typical in magmatic-hydrothermal system worldwide and is commonly used as indicator of magmatic-hydrothermal evolution (Jacamon and Larsen, 2009; Müller *et al.*, 2002; Breiter *et al.*, 2012, 2017). Thus, the Ge/Ti ratio provides a reliable index to track and unravel magmatic-hydrothermal transition in the mineralized system of Panasqueira. The Al, Li, Rb and B *vs.* Ge/Ti diagrams (Figs. 10d–10g) show that the magmatic-hydrothermal evolution of Panasqueira defined by increase of Ge/Ti ratio in quartz, is marked by a progressive depletion in Al, Li and Rb and by a progressive enrichment in B from magmatic quartz composing the two-mica granite to hydrothermal quartz from greisen and mineralized veins. In these different chemical trends, quartz composing greisen exhibits intermediate compositions that overlap both compositions of magmatic quartz from the two-mica granite and hydrothermal quartz from veins. This overlap is probably caused by the occurrences of relictual magmatic quartz in the greisen (like snowball quartz) and the crystallization of

neoformed quartz equilibrated with hydrothermal mineralizing fluids during greisenization.

7.3 Results of PERMANOVA

Results of PERMANOVA performed on the elemental compositions (Li, B, Na, Al, Ti, Ge, Rb, S, As and Sb) of the different populations of quartz are summarized in Table 2. Cores of snowball-textured quartz from the two-mica granite and greisen are strongly dissilimar to hydrothermal quartz occuring in greisen and in the mineralized veins. Rims of snowball-textured quartz and matrix quartz occuring in the two-mica granite are statistically undiscernable with an F-value of 0.56. This suggests that rims of snowball textured quartz and matrix quartz of the two-mica granite have likely crystallized at the same time during the granite cooling. PERMANOVA show also similarities between the different populations of hydrothermal quartz composing the greisen. Matrix quartz of greisen and euhedral quartz occuring in the greisen porosity are undistinguishable with an F-value of 0.76. These results indicate that hydrothermal overgrowth of snowball-textured quartz, matrix quartz of greisen and euhedral quartz that occur in greisen porosity were equilibrated with the same hydrothermal fluid during greisenization. Hydrothermal quartz related to the QTS of the mineralized veins and hydrothermal quartz from greisen are characterized by similar signatures with F-values below 5. Finally, euhedral quartz of the greisen porosity is the most similar of quartz related to the MOSS of the mineralized veins with an F-value of 11.93.

8 Apatite U-Pb ages

In cathodoluminescence images, the primary magmatic apatite commonly displays homogeneous dark-grey luminescence (Fig. 11a). However, some grains were slightly altered along the grain boundaries and exhibit a secondary light-grey-luminescent rim (Fig. 11a). Thus, only the unaltered parts of apatite grains were considered for U-Pb dating of magmatic apatites.

During greisenization of the two-mica granite, the primary magmatic apatite was partially conserved within the massive greisen. Cathodoluminescence images permit to follow the progressive alteration and replacement of this apatite (Fig. 11b). When the alteration is partial, the primary dark-grey-luminescent apatite was replaced by brighter luminescent secondary apatite along the grain margins and along micro-fracture planes. Magmatic apatite most affected by hydrothermal alteration exhibits complex patchy-zoning textures consistent with a strong pervasive alteration related to greisenization (Fig. 11b). The occurrences of thin oscillatory zoning (hydrothermal overgrowth) that surrounded some altered grains emphasized that a second generation of hydrothermal apatite was formed during the hydrothermal stages (Fig. 11b). Unfortunately, the U-Pb dating of this second generation of apatite is impossible due to their high content in non-radiogenic lead.

Several generations of apatite can be distinguished in the mineralized veins of Panasqueira. Here we focus our intention on the first generation of apatite whose crystallization accompanied the formation of the muscovite selvage and marks the early stages of vein formation (MOSS) (Fig. 5a). Cathodoluminescence images of these hydrothermal apatite display oscillatory zoning corresponding to growth bands (Fig. 11c).

U-Pb analyses of magmatic apatite from the two-mica granite, altered magmatic apatite from greisen and hydrothermal apatite from mineralized veins are given in supplementary materials (ESM6) and are reported in Terra-Wasserburg diagrams (Figs. 11d–11f). The ages are provided with 2σ errors and are calculated with unforced discordias (*i.e.* initial common Pb values are unforced). All ages presented in the following were obtained from discordant data.

A total of 23 analyses performed on a dozen grains of primary magmatic apatite give a well-defined discordia with $^{207}Pb/^{206}Pb$ ratios ranging from 0.262 to 0.839 and with a well-defined lower intercept date of 296 ± 4 Ma (MSWD = 0.6, $n = 23$) (Fig. 11d).

For altered magmatic apatite observed in greisen, we performed 31 analyses distributed over 15 grains. Analyses display high contents in common Pb compared to magmatic apatite with $^{207}Pb/^{206}Pb$ ratios ranging from 0.533 to 0.839. The unforced discordia yields a lower intercept date of 292 ± 10 Ma (MSWD = 1.7, $n = 23$) (Fig. 11e). The hydrothermal overgrowths (oscillatory zoning) surrounding the altered magmatic apatite grains are only composed of common Pb (red ellipses) and therefore do not permit to determine a lower intercept date (Fig. 11e).

For hydrothermal apatite composing the veins selvages, we performed 22 analyses out of 12 grains. These analyses display $^{207}Pb/^{206}Pb$ ratios ranging from 0.353 to 0.650 and give an unforced intercept date of 295 ± 5 Ma (MSWD = 2.2, $n = 22$) (Fig. 11f).

9 Interpretation and discussion

9.1 Thermic evolution of the magmatic-hydrothermal system of Panasqueira from the TitaniQ thermometer

It is largely admitted that incorporation of Ti in quartz depends strongly on (i) the activity of Ti (a_{TiO2}) in the melt-fluids, (ii) pressure conditions and (iii) on temperature conditions (Huang and Audétat, 2012; Thomas *et al.*, 2010; Wark and Watson, 2006). From experimental data and thermodynamic studies, several calibrations permitting to estimate temperature of quartz crystallization from Ti concentration were proposed (Wark and Watson, 2006; Thomas *et al.*, 2010; Huang and Audétat, 2012). Here, we apply the equation defined by Thomas *et al.* (2010) to estimate temperatures of crystallization for the different generations of quartz analyzed. For this calculation, we consider a pressure of 1 and 2 kbar according to values estimated by Bussink (1984) from fluid inclusions. Petrographic study provided evidence of occurrences of rutile in greisen and within mineralized veins associated to tourmaline (Carocci *et al.*, 2018). However, due to the difficulty to determine if these different populations of quartz and rutile are cogenetic, we consider values of a_{TiO2} ranging from 0.2 to 1 for calculations (Fig. 12).

Calculations performed with Ti activity (a_{TiO_2}) of 0.2 give relatively high crystallization temperatures for magmatic

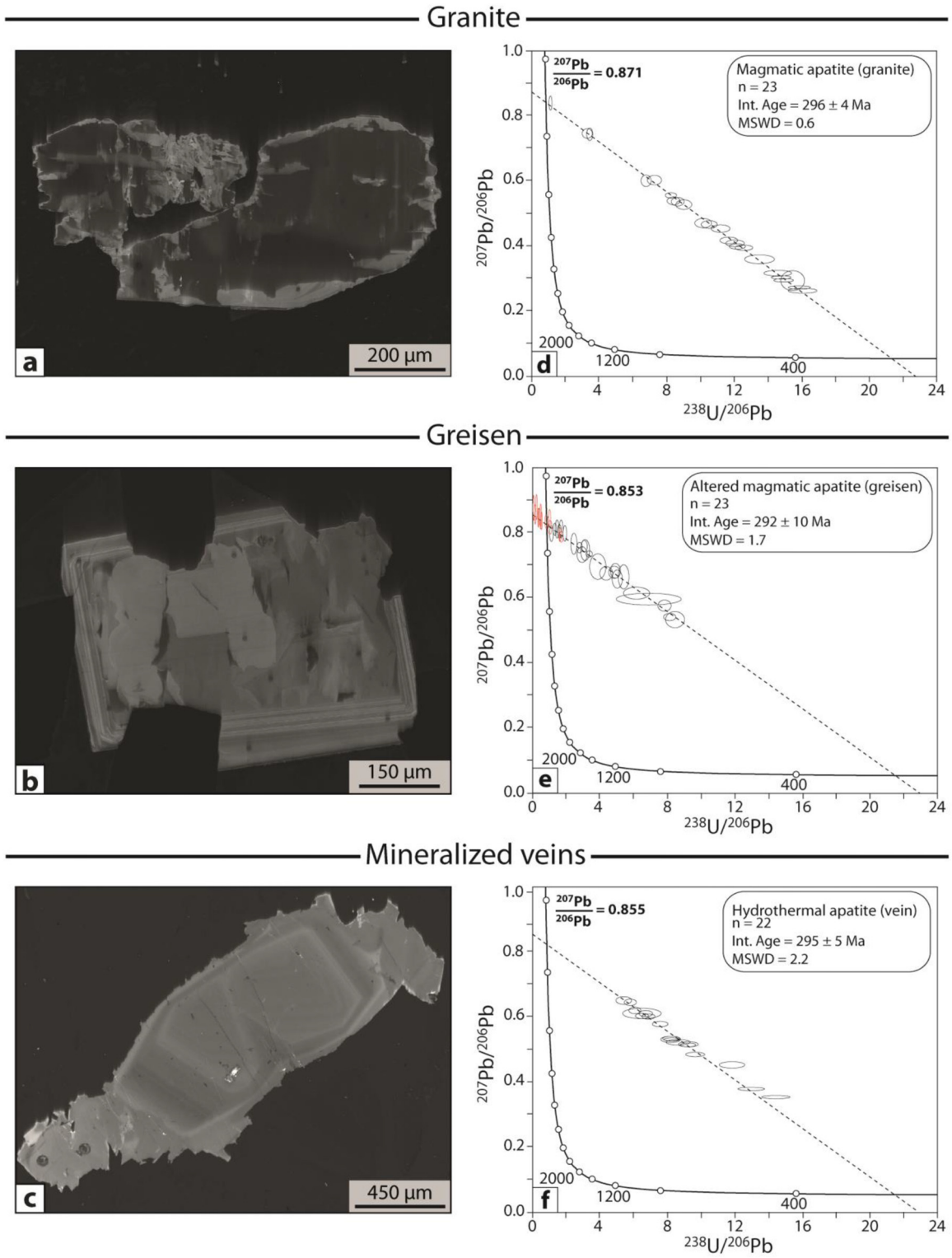

Fig. 11. (a) to (c) Representative cathodoluminescence images of (a) magmatic apatite from two mica granite, (b) altered magmatic apatite from greisen and (c) hydrothermal apatite from mineralized vein selvages. (d) to (e) Tera-Wasserburg concordia diagrams, in which apatite analyses were reported to define lower intercept date. (d) Results obtained for magmatic apatite from the unaltered two-mica granite. (e) Results obtained for altered magmatic apatite from greisen. Black ellipses correspond to analyses of altered magmatic apatite and red ellipses correspond to hydrothermal oscillatory zoning overgrowth (f) Results obtained for hydrothermal apatite from mineralized veins (veins selvages). The black dashed lines represent the unforced discordias used for age determination, the $^{207}Pb/^{206}Pb$ values obtained from the upper intersect of discordias are also indicated. Ellipses and errors on ages are reported at 2σ.

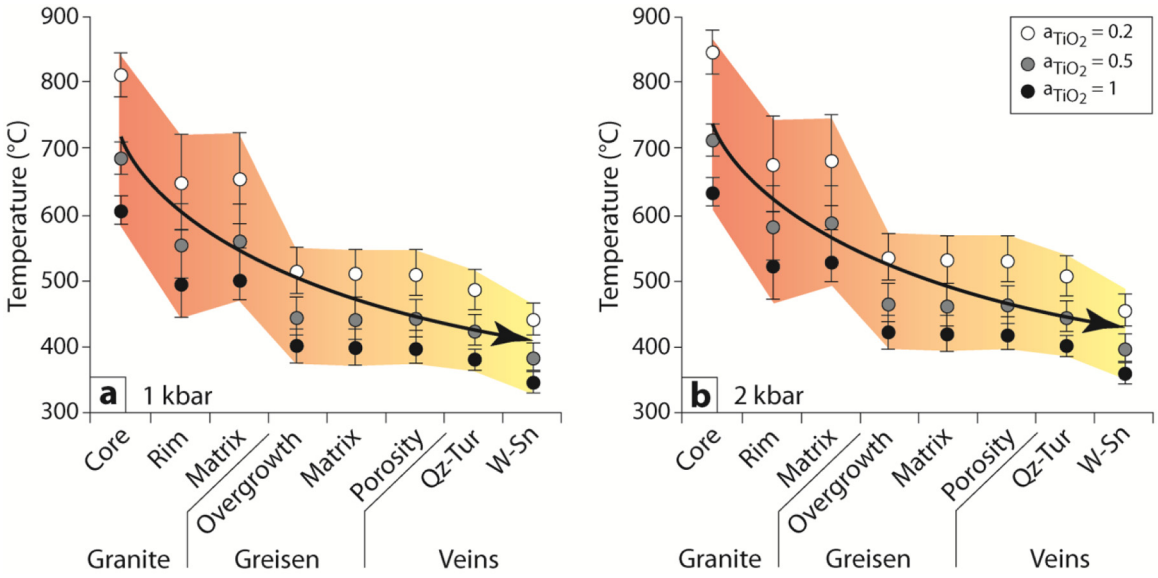

Fig. 12. Temperatures of quartz crystallization obtained for the different generations of magmatic and hydrothermal quartz of the unaltered two-mica granite, greisen and mineralized veins. Temperatures were obtained by applying the TitaniQ geothermometer defined by Thomas *et al.* (2010) at (a) 1 and (b) 2 kbar for Ti activity ranging from 0.2 to 1.

snowball-textured quartz (800 and 850 °C, at respectively 1 and 2 kbar) that are inconsistent with classical crystallization temperatures of granitic melts. Conversely, calculations performed with Ti activity of 0.5 and 1 for magmatic quartz give temperatures ranging between 600 and 700 °C, which are more consistent with temperatures of granite crystallization (Tuttle and Bowen, 1958; Luth *et al.*, 1964; Ackerson *et al.*, 2018). Ranges of crystallization temperatures calculated for rims of snowball-textured quartz and for the matrix quartz of the two-mica granite are similar (500–600 °C) (Fig. 12). Accordingly, these two populations of quartz crystallized contemporaneously and later than cores of snowball quartz. Considering a pressure of 1 kbar, hydrothermal quartz formed during the greisenization and the quartz-tourmaline stage (*i.e.* the earliest stage of veins formation) exhibits the same temperature ranges (400–500 °C) (Fig. 12). Quartz related to the W-Sn mineralization stage of veins is characterized by colder crystallization temperatures, which range between 350 and 450 °C (at 1 kbar). These crystallization temperatures are compatible with temperatures range in greisen systems worldwide (Smith *et al.*, 1996; Conliffe and Feely, 2006; Audétat *et al.*, 2008) and with temperatures obtained from fluid inclusions and boron isotopes exchange thermometry for the earliest hydrothermal stages of veins (Kelly and Rye, 1979; Bussink, 1984; Noronha *et al.*, 1992; Lüders, 1996; Codeço *et al.*, 2019). Finally, temperatures depict a cooling trend from magmatic quartz of granite to hydrothermal quartz of greisen and veins. This cooling trend is consistent with the expected thermic evolution of magmatic-hydrothermal systems and suggests a continual transition between magmatic (*i.e.* granite emplacement) and hydrothermal processes (*i.e.* greisenization and W-Sn-bearing quartz veins).

9.2 Spatiotemporal connection between granite cooling, greisenization and ore-bearing quartz veins

Experimental and empirical studies have demonstrated that the closure temperature of apatite range from 375 to 550 °C (Chamberlain and Bowring, 2001; Schoene and Bowring, 2006; Cochrane *et al.*, 2014). Consequently, U-Pb dating of apatite represents a good tool to constrain ages of cooling for large and polyphased intrusive bodies and ages of emplacement for small intrusive bodies like dyke and aplite (Pochon *et al.*, 2016). In addition, apatite is highly reactive during fluid-rock interactions (Harlov *et al.*, 2005; Bouzari *et al.*, 2016) and hence constitutes a good tool to date hydrothermal events and metasomatic processes related to greisenization. The granite cooling stage dated at 296 ± 4 Ma by U-Pb dating of magmatic apatites overlaps the formation of the vein selvages, which was dated at 295 ± 5 Ma by U-Pb dating of hydrothermal apatite and 296 ± 0.6 Ma by Ar-Ar dating of muscovite-rich selvages (Snee *et al.*, 1988). U-Pb apatite age (292 ± 10 Ma) for greisenization is within errors identical to ages obtained for veins and granite cooling. Accordingly, greisenization and the formation of W-Sn-bearing quartz veins of were coeval with crystallization and cooling of the Panasqueira two-mica granite present at depth. Furthermore, hydrothermal activity related to the sulphides mineralization of veins dated at 294 ± 0.9 Ma (by Ar-Ar dating of late muscovite, Snee *et al.*, 1988) appears to be in direct continuity with the granite cooling and the W-Sn mineralization stage. Consequently, the different hydrothermal stages observed in the mineralized veins of Panasqueira were related to the same thermic event, which was likely controlled by the cooling of the granite intrusion. The overlapping ages of the granite cooling, greisenization and the W-Sn mineralized quartz veins, in combination with strong spatial relationships argue in favor of

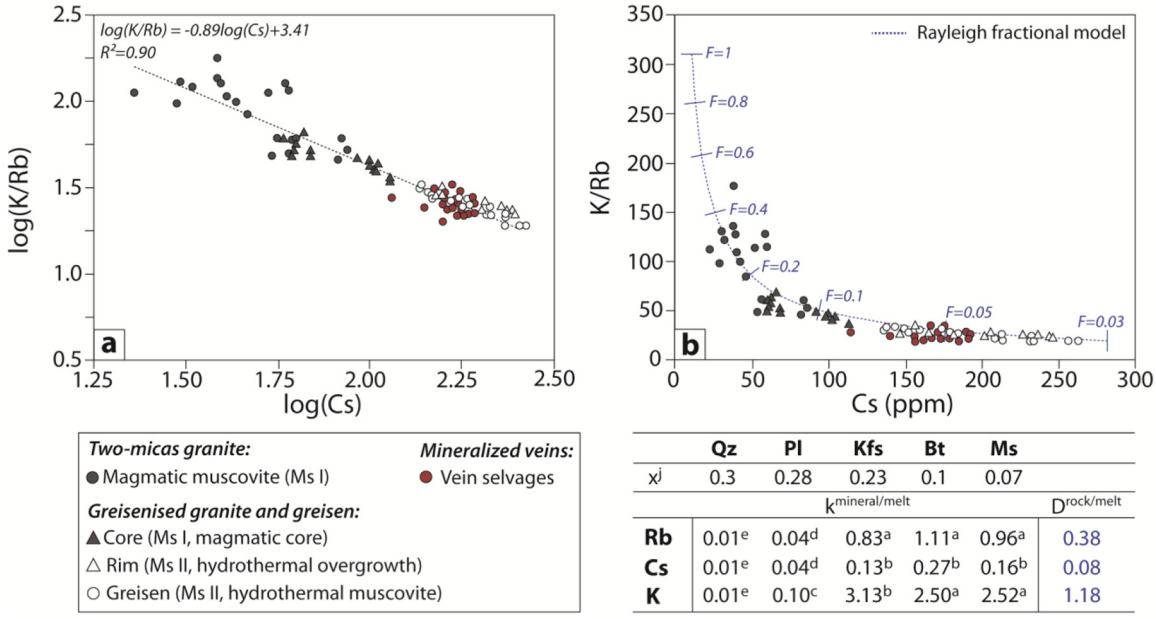

	Qz	Pl	Kfs	Bt	Ms	
x^j	0.3	0.28	0.23	0.1	0.07	
	$k^{mineral/melt}$					$D^{rock/melt}$
Rb	0.01[e]	0.04[d]	0.83[a]	1.11[a]	0.96[a]	0.38
Cs	0.01[e]	0.04[d]	0.13[b]	0.27[b]	0.16[b]	0.08
K	0.01[e]	0.10[c]	3.13[b]	2.50[a]	2.52[a]	1.18

Fig. 13. (a) log(K/Rb) *versus* log(Cs) relationship in muscovite composing granite, greisen and the mineralized veins of Panasqueira. (b) Modelled compositional evolution trend of muscovite formed during fractional crystallization of the Panasqueira granite (*F* gives the fraction of remaining liquid). This trend is calculated applying the Rayleigh equation $C_i^{Ms} = k_{d,i}^{Ms/melt} * C_{0,i}^{Liq} * F^{(D_i-1)}$ (Hulsbosch *et al.*, 2014) and assuming a starting composition of granitic melt ($C_{0,i}^{Liq}$) of 370 ppm Rb, 70 ppm Cs and 44 900 ppm K. Modal proportion of minerals (x^j) composing the Panasqueira two-mica granite and mineral/melt partition coefficients ($k_{d,i}^j$) for K, Rb and Cs used for calculation of distribution coefficients (*Di*) are summarized in table below diagram b. References for k_d: [a]Icenhower and London (1996); [b]Icenhower and London (1995); [c]Philpotts and Schnetzler (1970); [d]Jolliff *et al.* (1992); [e]Nash and Crecraft (1985).

the involvement of the Panasqueira two-mica granite during the formation of the ore-bearing quartz veins. Additionally, the occurrences of disseminated cassiterite and scarce wolframite in greisen, as well as enrichment of greisen in ore metals (W and Sn) compared to the Panasqueira two-mica granite support that greisenization is coeval to vein formation and results from the ingress of W-Sn-rich fluids through the apical part of the granitic intrusion.

9.3 Chemical characteristics of fluids related to greisenization and veins

Composition of quartz-muscovite assemblages depend on temperature, pressure, composition of melt-fluids and crystal-melt or crystal-fluid partitioning coefficients. In the following, major and trace elements variations in quartz-muscovite assemblages are used as tracers of magmatic-hydrothermal processes and to decipher geochemistry of hydrothermal fluids related to greisenization and the formation of mineralized veins.

Compositions of quartz-muscovite assemblages from greisen and mineralized veins demonstrate that fluids related to greisenization and the earliest stages of vein formation were rich in granophile elements (F, Li, Rb, Cs and B) and ore metals (W, Sn and Zn). These results are consistent with direct analysis of quartz-hosted fluid inclusions from mineralized veins performed by Lecumberri-Sanchez *et al.* (2017). They demonstrated that fluids related to the W-Sn mineralization of Panasqueira are significantly enriched in (i) B, Li, Cs and Rb with concentrations up to several hundred of ppm and (ii) ore metals (W, Cu and Zn) with concentrations reaching several tens or hundreds of ppm. The multivariate statistical treatments (PCA and PERMANOVA) performed on trace elements compositions of quartz and muscovite demonstrated that quartz-muscovite assemblages from greisen and ore-bearing quartz veins have statistically close signatures. This implies a genetic link between greisenization and the formation of W-Sn-bearing quartz veins that result likely from circulation of same fluids.

9.3.1 Incorporation of trace elements in quartz and interpretation of chemical trends

The most significant variations in trace element contents observed in quartz mainly concern Al, Ti, Li, Rb, Ge and B. As discussed previously, incorporation of Ti in quartz is partly dependent on temperature conditions. The progressive decrease of Ti content observed from magmatic to hydrothermal quartz reflects directly the progressive cooling of the magmatic hydrothermal system of Panasqueira.

Germanium is compatible in quartz and its incorporation is primarily controlled by the amount of Ge present in melt/fluid. In magmatic system, the increase in Ge contents is a robust indicator of magma fractionation (Larsen *et al.*, 2004; Müller *et al.*, 2010; Breiter *et al.*, 2017; Monnier *et al.*, 2018). Indeed, Ge is preferentially concentrated in residual melt and fluids, explaining the higher Ge contents observed in quartz composing evolved granites and hydrothermal veins. Herein, the enrichment

in Ge observed in hydrothermal quartz from greisen and ore-bearing quartz veins suggest that greisenization and the formation of mineralized veins result from the circulation of magmatic fluids, in which Ge was concentrated during the progressive crystallization of the Panasqueira granite.

Li and Rb are generally considered as incompatible elements, which were preferentially concentrated in residual melt and magmatic fluids. Accordingly, hydrothermal quartz from greisen and mineralized veins should be richer in Li and Rb than magmatic quartz. However, compositional evolutions of quartz show the opposite trend. This contradiction can be attributed to (i) the crystallization of a large amount of muscovite both in greisen and within the mineralized veins that incorporate preferentially these elements and (ii) a limited incorporation of Al in hydrothermal quartz that consequently inhibits the incorporation of Li according to the coupled substitution Li Al↔Si. Although, the high Rb and Li contents in hydrothermal muscovite of greisen and veins support the first hypothesis, the low Al contents in hydrothermal quartz and the Li-Al correlation observed previously seem to confirm the second assumption.

The B enrichment from magmatic quartz to hydrothermal quartz of veins is consistent with the incompatible behavior of B that is preferentially concentrated in residual melt and tends to be expelled with magmatic fluids (Pichavant, 1981; London *et al.*, 1988). The circulation of these B-rich fluids resulting from crystallization of the Panasqueira granite explain the intense tourmalinization of metasedimentary host rock observed around veins as well as the crystallization of tourmaline at the incipient stage of vein formation (Codeço *et al.*, 2017; Launay *et al.*, 2018; Carocci *et al.*, 2018).

9.3.2 Evidences for magmatic fluid exsolution

Hydrothermal muscovite from greisen and ore-bearing quartz veins are enriched in fluid mobile granophile elements (F, Li, Rb, Cs, Sn and W) suggesting involvement of magmatic contributions. Alkali metal (Li, Rb and Cs) are commonly used as differentiation proxies for pegmatite and W-Sn mineralized veins systems (Neiva, 1987; Černý *et al.*, 2005; Hulsbosch *et al.*, 2014, 2016). Indeed, during fractional crystallization, these incompatible elements get enriched in residual granitic melt and successively in orthomagmatic fluids exsolved during the final consolidation of granitic intrusion. Although muscovite from greisen and veins are hydrothermal origin, their compositions define a good linear trend with magmatic muscovite in log(K/Rb) *versus* log(Cs) representation (Fig. 13a). According to Hulsbosch *et al.* (2014) this linear relationship constitutes a robust argument to demonstrate involvement of Rayleigh fractional crystallization process in magmatic-hydrothermal systems. Here, this seems to confirm that muscovite composing greisen and the W-Sn bearing quartz veins crystallized from magmatic fluids, which were equilibrated with residual granitic melt during the final stage of magmatic–hydrothermal differentiation of the Panasqueira two-mica granite. Furthermore, compositions of magmatic and hydrothermal muscovite appear to be consistent with the theoretical compositional evolution trend of muscovite predict by Rayleigh fractional crystallisation model of the Panasqueira two-mica granite (blue dashed line in Fig. 13b). This supports that fractional crystallization of the Panasqueira granite is the most likely process for production of fluids enriched in granophile elements recorded by hydrothermal muscovite. Herein, we propose that greisenization and the formation of ore-bearing veins result from the exsolution of magmatic W-Sn bearing fluids during the magmatic-hydrothermal transition, which marks the final stage of fractional crystallization of the Panasqueira granite. The fluid flow pattern determined by Launay *et al.*, (2018) at the magmatic-hydrothermal transition, as well as boron isotopic composition of tourmalines from veins realized by Codeço *et al.*, 2017 support this interpretation.

9.4 Genetic relationship between greisenization and W-Sn mineralization

As highlighted from (i) temperature evolution constrained from quartz geothermometry, (ii) geochemical signature of fluids deduced from quartz and muscovite compositions and (iii) U-Pb apatite geochronology, greisenization and the formation of the mineralized veins are coeval and result likely from the exsolution of orthomagmatic W-Sn-bearing fluids. The concomitant formation of mineralized veins and greisen was already proposed by Korges *et al.* (2018) for the Zinnwald Sn-W deposit. According to this study Sn-greisen formation and precipitation of quartz-Sn-W veins result from the exsolution and the depressurization of a single magmatic-hydrothermal fluid released during the progressive cooling of the deeper granite intrusion. Herein, to illustrate the interplay between fluids produced during the late stage of fractional crystallization of the Panasqueira granite and greisenization, we propose a conceptual model based on the disequilibrium between hot acidic magmatic fluids released at high temperature and cooler crystallized part of the granite intrusion (Fig. 14). If we consider that albite, k-feldspar and muscovite are equilibrated during the final stages of the granite crystallization (eutectic), the composition of magmatic fluids in $log(a_{Na^+}/a_{H+})$ and $log(a_{K^+}/a_{H+})$ released by the granite is constrained by the triple point at high temperature conditions (red star at 600 °C in Fig. 14). The exsolution and the circulation of these fluids through the cooler and crystallized part of the intrusive body trigger the replacement of feldspars (k-feldspar and albite) by muscovite due to disequilibrium induced by the temperature differences between hot-acidic magmatic fluids (600 °C in Fig. 14) and crystallized granite (400 °C in Fig. 14). During the hydrolysis of feldspars and biotite, the neoformed muscovite and quartz record the chemical signature of fluids that were enriched in granophile elements and metals, whereas elements hosted by feldspars (Na, Ba, Sr, Eu...) were released in fluids. The crystallization of a large amount of muscovite and quartz and chemical exchanges between these minerals and fluids explain the Cs, Rb, Li enrichment and Na, Ba and Sr depletion observed in the whole-rock composition during greisenization. Reactions of feldspar replacement in quartz-muscovite assemblage consume acidity of mineralized fluids. This fluid neutralization can induce a Sn solubility decrease and thus cassiterite crystallization (Heinrich, 1990) that explain the occurrences of cassiterite in greisen porosity. Then, the W-Sn bearing fluids flowed through the vein network during earliest mineralization stages (QTS and

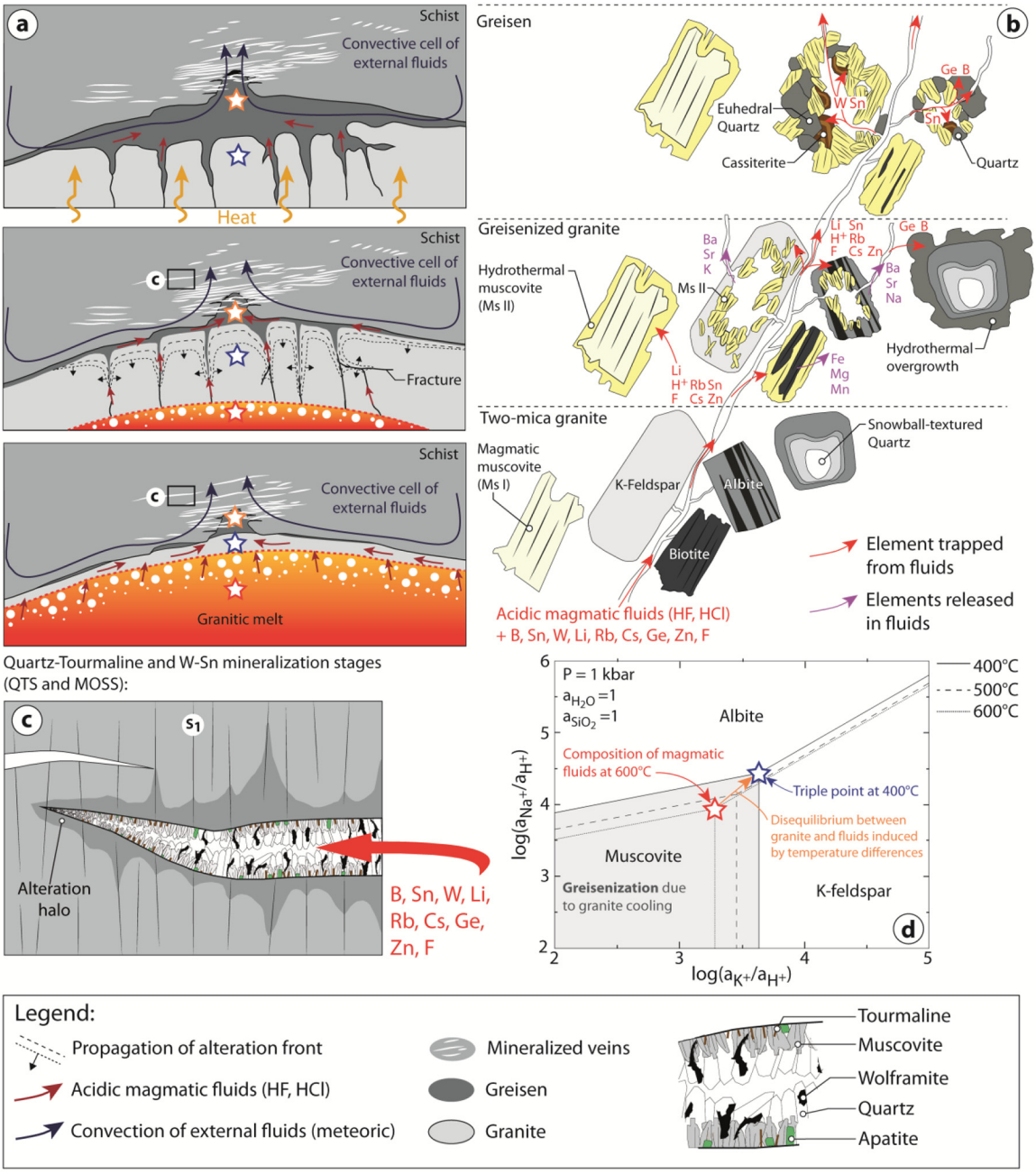

Fig. 14. Conceptual model of greisen formation during the magmatic-hydrothermal transition of Panasqueira. In this model are displayed (a) the schematic time evolution of fluid flow during the granite crystallization and cooling, (b) the textural and the mineralogical evolution of granite with the behavior of some elements considered in this study, (c) zoom on mineralized veins related to QTS and MOSS and (d) $log(a_{Na^+}/a_{H^+})$ *vs.* $log(a_{K^+}/a_{H^+})$ phases diagram at 1 kbar illustrating effect of temperatures (from 600 to 400 °C) on equilibria between K-feldspar, albite and muscovite. Triple point corresponds to hypothetic eutectic of the two-mica granite of Panasqueira. During granite cooling, fluid produced at high magmatic temperature (red star) is imbalance with the cooler crystallized part of the granite intrusion that potentially trigger greisenization. This diagram was built from thermodynamic database of SUPCRTBL (Johnson *et al.*, 1992; Zimmer *et al.*, 2016).

MOSS) that triggered the opening and the formation of the mineralized veins (Foxford *et al.*, 2000; Launay *et al.*, 2018). In these veins, the muscovite-rich selvages and quartz record the same chemical signature of fluids than quartz-muscovite assemblage composing greisen. As demonstrated by Lecumberri-Sanchez *et al.*, (2017), interactions between W-Sn-bearing fluids and metasedimentary host rocks caused strong alteration along vein margins (tourmalinization and muscovitization) that triggers Fe leaching from schist and hence crystallization of wolframite in mineralized veins.

Acknowledgments. This research took part in the ERAMIN project "New Ores" (ANR-14-EMIN-0001) and was

financially supported by the French Geological Survey (BRGM), the Region Centre, and the Labex Voltaire (ANR-10-LABX-100-01).

References

Ackerson M, Mysen BO, Tailby N, Watson E. 2018. Low-temperature crystallization of granites and the implications for crustal magmatism. *Nature* 559. https://doi.org/10.1038/s41586-018-0264-2.

Alfonso P, Melgarejo JC, Yusta I, Velasco F. 2003. Geochemistry of feldspars and muscovite in granitic pegmatite from the Cap de Creus field, Catalonia, Spain. *The Canadian Mineralogist* 41: 103–116.

Anderson MJ. 2001. A new method for non-parametric multivariate analysis of variance. *Austral Ecology* 26: 32–46.

Audétat A, Pettke T, Heinrich CA, Bodnar RJ. 2008. Magmatic-hydrothermal evolution in a fractionating granite: a microchemical study of the Sn-W-F mineralized Mole granite (Australia). *Geochim Cosmochim Acta* 64: 3373–3393.

Azor A, Dias da Silva Í, Gómez Barreiro J, González-Clavijo E, Martínez Catalán JR, Simancas JF, *et al.* 2019. Deformation and Structure. In: Quesada C, Oliveira JT, eds. *The Geology of Iberia: A Geodynamic Approach: Vol. 2: The Variscan Cycle, Regional Geology Reviews*. Cham: Springer International Publishing, pp. 307–348. https://doi.org/10.1007/978-3-030-10519-8_10.

Ballouard C, Branquet Y, Tartese R, Poujol M, Boulvais P, Vigneresse J-L. 2016. Nb-Ta fractionation in peraluminous granites: A marker of the magmatic hydrothermal transition – REPLY. *Geology* 44: e395. https://doi.org/10.1130/G38169Y.1.

Belissont R, Boiron MC, Luais B, Cathelineau M. 2014. LA-ICP-MS analyses of minor and trace elements and bulk Ge isotopes in zoned Ge-rich sphalerites from the Noailhac-Saint-Salvy deposit (France): insights into incorporation mechanisms and ore deposition processes. *Geochim. Cosmochim. Ac.* 126: 518–540.

Bishop AC. 1989. Greisen. In: *Petrology. Encyclopedia of Earth Science*. Boston, MA: Springer.

Bouzari F, Hart CJR, Bissig T, Barker S. 2016. Hydrothermal Alteration Revealed by Apatite Luminescence and Chemistry: A Potential Indicator Mineral for Exploring Covered Porphyry Copper Deposits. *Economic Geology* 111: 1397–1410.

Breiter K, Müller A, Leichmann J, Gabašová A. 2005. Textural and chemical evolution of a fractionated granitic system: the Podlesí stock, Czech Republic. *Lithos* 80: 323–345.

Breiter K, Svojtka M, Ackerman L, Švecová K. 2012. Trace element composition of quartz from the Variscan Altenberg-Teplice caldera (Krušné hory/Erzgebirge Mts, Czech Republic/Germany): insights into the volcano-plutonic complex evolution. *Chem. Geol.* 326-327: 36–50.

Breiter K, Ďurišová J, Dosbaba M. 2017. Quartz chemistry – A step to understanding magmatic-hydrothermal processes in ore-bearing granites: Cínovec/Zinnwald Sn-W-Li deposit, Central Europe. *Ore Geology Reviews* 90: 25–35.

Breiter K, Hložková M, Korbelová Z, Vasinova Galiova M. 2019. Diversity of lithium mica compositions in mineralized granite–greisen system: Cínovec Li-Sn-W deposit, Erzgebirge. *Ore Geology Reviews* 106. https://doi.org/10.1016/j.oregeorev.2019.01.013.

Bussink RW. 1984. Geochemistry of the Panasqueira Tungsten-Tin Deposit, Portugal. *Geol. Ultraiectina*.

Carocci E, Marignac C, Cathelineau M, Truche L, Lecomte A, Pinto F. 2018. Rutile from Panasqueira (Central Portugal): An Excellent Pathfinder for Wolframite Deposition. *Minerals* 9: 9. https://doi.org/10.3390/min9010009.

Castro A, Corretgé GL, De La Rosa J, Enrique P, Martínez FJ, Pascual E, *et al*. 2002 Palaeozoic Magmatism. In: Gibbons W, Moreno MT, eds. *The Geology of Spain*. London: Geological Society, pp. 117–53.

Černý P, Blevin PL, Cuney M, London D. 2005. Granite-Related Ore Deposits. In: Hedenquist JW, Thompson JFH, Goldfarb RJ, Richards JR, eds. *Economic Geology – One Hundredth Anniversary Volume*, pp. 337–370.

Chamberlain KR, Bowring SA. 2001. Apatite-feldspar U-Pb thermochronometer: a reliable, mid-range (~450 °C), diffusion controlled system. *Chemical Geology* 172: 173–200.

Charoy B, Noronha F. 1991. The Argemela granite-porphyry (Central Portugal): The subvolcanic expression of a high-fluorine, rare-element pegmatite magma. In Leroy P, ed. *Source, Transport and Deposition of Metals*. Balkema, Rotterdam. ISBN 9054100206.

Clark AH. 1964. Preliminary study of the temperatures and confining pressures of granite emplacement and mineralization, Panasqueira, Portugal. *Inst. Mining MetallurgyTrans.* 73: 813–824.

Cochrane R, Spikings RA, Chew D, Wotzlaw J-F, Chiaradia M, Tyrrell S, *et al*. 2014. High temperature (> 350 °C) thermochronology and mechanisms of Pb loss in apatite. *Geochimica et Cosmochimica Acta* 127: 39–56.

Codeço M, Weis P, Trumbull R, Pinto F, Lecumberri-Sanchez P, Wilke F. 2017. Chemical and boron isotopic composition of hydrothermal tourmaline from the Panasqueira W-Sn-Cu deposit, Portugal. *Chemical Geology* (online).

Codeço MS, Weis P, Trumbull RB, Glodny J, Wiedenbeck M, Romer RL. 2019. Boron-isotope muscovite-tourmaline geothermometry indicates fluid cooling during magmatic-hydrothermal W-Sn-ore formation. *Economic Geology* 114(1): 153–163. https://doi.org/10.5382/econgeo.2019.4625.

Conliffe J, Feely M. 2006. Microthermometrics characteristics of fluids associated with granite and greisen quartz and vein quartz and beryl from Rosses Granite complex, Donegal, NW Ireland. *J Geochem Explor* 89: 73–77.

Dias G, Leterrier J, Mendes A, Simões P, Bertrand JM. 1998. U-Pb zircon and monazite geochronology of syn- to post-tectonic Hercynian granitoids from the central Iberian Zone (northern Portugal). *Lithos* 45: 349–369.

Dolejs D. 2015. Quantitative characterization of hydrothermal systems and reconstruction of fluid fluxes: the significance of advection, disequilibrium, and dispersion. In: *SGA Proceedings 13th SGA Biennial Meeting*.

Dostal J, Kontak DJ, Ochir G, Shellnutt J, Fayek M. 2015. Cretaceous ongonites (topaz-bearing albite-rich microleucogranites) from Ongon Khairkhan, Central Mongolia: Products of extreme magmatic fractionation and pervasive metasomatic fluid: Rock interaction. *Lithos* 236-237: 173–189.

Foxford KA, Nicholson R, Polya DA. 1991. Textural evolution of W-Cu-Sn bearing hydrothermal quartz veins at Minas da Panasqueira, Portugal. *Mineralogical Magazine* 55: 435–445.

Foxford KA, Nicholson R, Polya DA, Hebblethwaite RPB. 2000. Extensional failure and hydraulic valving at Minas da Panasqueira, Portugal: Evidence from vein spatial distributions, displacements and geometries. *J. Struct. Geol.* 22: 1065–1086.

Gomes M, Neiva A. 2000. Chemical zoning of muscovite from the Ervedosa granite, northern Portugal. *Mineralogical Magazine* 64: 347–358. https://doi.org/10.1180/002646100549247.

Götze J, Plötze M, Graupner T, Hallbauer DK, Bray CJ. 2004. Trace element incorporation into quartz: a combined study by ICP-MS, electron spin resonance, cathodoluminescence, capillary ion analysis, and gas chromatography 1. *Geochimica et Cosmochimica Acta* 68: 3741–3759.

Grant JA. 1986. The isocon diagram; a simple solution to Gresens' equation for metasomatic alteration. *Economic Geology* 81(8): 1976–1982.

Guidotti CV. 1984. Micas in metamorphic rocks. In: Bailey SW, ed. *Micas*. Washington: Mineralogical Society of America, pp. 357–467.

Gurbanov AG, Chernukha DG, Koshchug DG, Kurasova SP, Fedyushchenko SV. 1999. EPR spectroscopy and geochemistry of rock-forming quartz as an indicator of the superimposed processes in rocks of igneous associat ions of various ages in the Greater Caucasus. *Geochem. Int.* 37: 519–604.

Hammer H, Harper D, Ryan PPD. 2001. PAST: Paleontological Statistics software package for education and data analysis. *Palaeontologia Electronica* 4: 9.

Harlov DE, Wirth R, Förster HJ. 2005. An experimental study of dissolution–reprecipitation in fluorapatite: fluid infiltration and the formation of monazite. *Contrib Mineral Petr* 150: 268–286.

Heaney PJ, Veblen DR, Post JE. 1994. Structural disparities between chalcedony and macrocrystalline quartz. *American Mineralogist* 79: 452–460.

Hebblethwaite RPB, Antao AM. 1982. A report on the study of dilation patterns within the Panasqueira ore body: Barroca Grande, Beralt Tin Wolfram (Portugal), unpub. rept., 15 p.

Heinrich CA. 1990. The chemistry of hydrothermal tin – tungsten ore deposits. *Econ. Geol.* 85: 457–481.

Huang R, Audétat A. 2012. The titanium-in-quartz (TitaniQ) thermobarometer: A critical examination and re-calibration. *Geochimica et Cosmochimica Acta* 84: 75–89.

Hulsbosch N, Hertogen J, Dewaele S, André L, Muchez P. 2014. Alkali metal and rare earth element evolution of rock-forming minerals from the Gatumba area pegmatites (Rwanda): quantitative assessment of crystal-melt fractionation in the regional zonation of pegmatite groups. *Geochim. Cosmochim. Acta* 132: 349–374.

Icenhower J, London D. 1995. An experimental study of element partitioning among biotite, muscovite, and coexisting peraluminous silicic melt at 200 MPa (H2O). *Am. Mineral.* 80: 1229–1251.

Icenhower J, London D. 1996. Experimental partitioning of Rb, Cs, Sr, and Ba between alkali feldspar and peraluminous melt. *Am. Mineral.* 81: 719–734.

Jacamon F, Larsen RB. 2009. Trace element evolution of quartz in the charnockitic Kleivan granite, SW-Norway: the Ge/Ti ratio of quartz as an index of igneous differentiation. *Lithos* 107: 281–291.

Johnson JW, Oelkers EH, Helgeson HC. 1992. SUPCRT92–A software package for calculating the standard molal thermodynamic properties of minerals, gases, aqueous species, and reactions from 1-bar to 5000-bar and 0 to 1000 °C. *Computer and Geosciences* 18: 899–947.

Jolliff BL, Papike JJ, Shearer CK. 1992. Petrogenetic relationships between pegmatite and granite based on geochemistry of muscovite in pegmatite wall zones, Black Hills, South Dakota, USA. *Geochim. Cosmochim. Acta* 56: 1915–1939.

Julivert M, Fontboté JM, Ribeiro A, Conde L. 1972. Mapa Tectonico de la Peninsula Iberica y Baleares E. 1:1.000.000. *Inst. Geol. Min.*, España, Madrid.

Kaeter D, Barros R, Menuge J, Chew D. 2018. The magmatic-hydrothermal transition in rare-element pegmatites from southeast Ireland: LA-ICP-MS chemical mapping of muscovite and columbite-tantalite. *Geochimica et Cosmochimica Acta.* 240. https://doi.org/10.1016/j.gca.2018.08.024.

Kelly WC, Rye RO. 1979. Geologic, fluid inclusion and stable isotope studies of the tin-tungsten deposits of Panasqueira, Portugal. *Econ Geol* 74: 1721–1822.

Korges M, Weis P, Lüders V, Laurent O. 2018. Depressurization and boiling of a single magmatic fluid as a mechanism for tin-tungsten deposit formation. *Geology* 46(1): 75–78.

Kotlyar BB, Ludington S, Mosier DL. 1995, Descriptive, grade, and tonnage models for molybdenum-tungsten greisen deposits: U.S. Geological Survey, Open-File Report 95-584, 30 p.

Larsen RB, Henderson H, Ihlen PM, Jacamon F. 2004. Distribution and petrogenetic behaviour of trace elements in granitic pegmatite quartz from granite from South Norway. *Contributions to Mineralogy and Petrology* 147: 615–628.

Launay G. 2019. Dynamic permeability related to greisenization in Sn-W ore deposits: Quantitative petrophysical and experimental evidence. Geofluids 2019. https://doi.org/10.1155/2019/5976545.

Launay G, Sizaret S, Guillou-Frottier L, Gloaguen E, Pinto F. 2018. Deciphering fluid flow at the magmatic-hydrothermal transition: A case study from the world-class Panasqueira W-Sn-(Cu) ore deposit (Portugal). *Earth and Planetary Science Letters* 499: 1–12.

Lecumberri-Sanchez P, Vieira R, Heinrich CA, Pinto F, Wälle M. 2017. Fluid-rock interaction is decisive for the formation of tungsten deposits. *Geology* 45: 579–582.

Legros H, Marignac C, Mercadier J, Cuney M, Richard A, Wang R-C, *et al*. 2016. Detailed paragenesis and Li-mica compositions as recorders of the magmatic-hydrothermal evolution of the Maoping W-Sn deposit (Jiangxi, China). *Lithos* 264: 108–124.

Legros H, Marignac C, Tabary T, Mercadier J, Richard A, Cuney M, *et al*. 2018. The ore-forming magmatic-hydrothermal system of the Piaotang W-Sn deposit (Jiangxi, China) as seen from Li-mica geochemistry. *American Mineralogist.* 103: 39–54. https://doi.org/10.2138/am-2018-6196.

Lehmann B. 1990. Lehmann Metallogeny of tin. In: Lecture notes in *Earth Sciences* 32, Springer-Verlag, 211 p.

London, D, Hervig RL, Morgan VIGB. 1988. Melt – Vapor solubilities and elemental partitioning in peraluminous granite – Pegmatite systems: experimental results with Macusani glass at 200 MPa. *Contrib. Mineral. Petrol.* 99: 360–373.

Lüders V. 1996. Contribution of infrared microscopy to fluid inclusion studies in some opaque minerals (Wolframite, Stibnite, Bournonite): Metallogenic implications. *Economic Geology* 91(8): 1462–1468.

Ludwig KR. 2012. User's Manual for Isoplot 3.75. A geochronological toolkit for Microsoft Excel. Berkeley Geochronological Center, pp. 1–75.

Luhr JF, Carmichael ISE, Varecamp JC. 1984. The 1982 eruptions of El Chichon volcano, Chiapas, Mexico: mineralogy and petrology of the anhydrite-bearing pumices. *Journal of Volcanology and Geothermal Research* 76: 83–109.

Luth WC, Jahns RH, Tuttle OF. 1964. The granite system at pressures of 4 to 10 kilobars. *J. Geophys. Res.* 69(4): 759–773. https://doi.org/10.1029/JZ069i004p00759.

McDowell FW, McIntosh WC, Farley KA. 2005. A precise 40Ar–39Ar reference age for the Durango apatite (U–Th)/He and fission-track dating standard. *Chemical Geology* 214: 249–263.

Michaud JA-S, Gumiaux C, Pichavant M, Gloaguen E, Marcoux E. 2020. From magmatic to hydrothermal Sn-Li-(Nb-Ta-W) mineralization: The Argemela area (central Portugal). *Ore Geology Reviews* 116: 103215. https://doi.org/10.1016/j.oregeorev.2019.103215.

Migdisov AA, Williams-Jones AE. 2005. An experimental study of cassiterite solubility in HCl-bearing water vapour at temperatures up to 350 °C. Implications for tin ore formation. *Chemical Geology* 217: 29–40

Miller CF, Stoddard EF, Bradfish LJ, Dollase WA. 1981. Composition of plutonic muscovite: Genetic implications. *Can. Mineral.* 19: 25–34.

Monecke T, Kempe U, Götze J. 2002. Genetic significance of the trace element content in metamorphic and hydrothermal quartz:

a reconnaissance study. *Earth and Planetary Science Letters* 202: 709–724.
Monier G, Robert J-L. 1986. Evolution of the miscibility gap between muscovite and biotite solid solutions with increasing lithium content: an experimental study in the system K2O-Li2O-MgO-FeO-Al2O3-SiO2-H2O-HF at 600°, 2 kbar PH2O: comparison with natural lithium micas. *Mineralogical Magazine* 50: 641–651.
Monier G, Merggoil-Daniel J, LabernardieÁre H. 1984. GeÂneÂrations successives de muscovites et feldspaths potassiques dans les leucogranites du massif de Millevaches (Massif Central Francais). *Bull. Mineral.* 107: 55–68.
Monnier L, Lach P, Salvi S, Melleton J, Bailly L, Béziat D, *et al*. 2018. Quartz trace-element composition by LA-ICP-MS as proxy for granite differentiation, hydrothermal episodes, and related mineralization: The Beauvoir Granite (Echassières district), France. *Lithos* 320-321: 355–377.
Monnier L, Salvi S, Melleton J, Bailly L, Béziat D, Parseval P, *et al*. 2019. Multiple Generations of Wolframite Mineralization in the Echassieres District (Massif Central, France). *Minerals* 9: 637. https://doi.org/10.3390/min9100637.
Mlynarczyk M, Sherlock R, Williams-Jones A. 2002. San Rafael, Peru: Geology and structure of the worlds richest tin lode. *Mineralium Deposita* 38: 555–567.
Müller A, Seltmann R. 1999. The genetic significance of snowball quartz in high fractionated tin granites of the Krušné Hory/Erzgebirge. In: Stanley C, ed. *Mineral Deposits: Processes to Processing*. *Proceedings of the 5th Biennial SGA Meeting London*, vol. 1, Balkema, Rotterdam, pp. 409–412.
Müller A, Kronz A, Breiter K. 2002. Trace elements and growth patterns in quartz: a fingerprint of the evolution of the subvolcanic Podlesí Granite System (Krušné Hory, Czech Republic). *Bulletin of the Czech Geological Survey* 77: 135–145.
Müller A, van den Kerkhof AM, Behr H-J, Kronz A, Koch-Müller M. 2010. The evolution of late-Hercynian granites and rhyolites documented by quartz – A review. *Geol. Soc. Am. Spec. Pap.* 472: 185–204.
Müller A, Herklotz G, Giegling H. 2018. Chemistry of quartz related to the Zinnwald/Cínovec Sn-W-Li greisen-type deposit, Eastern Erzgebirge, Germany. *Journal of Geochemical Exploration* 190: 357–373.
Nash WP, Crecraft HR. 1985. Partition coefficients for trace elements in silicic magmas. *Geochimica et Cosmochimica Acta* 49: 2309–2322.
Neiva AMR. 1987. Geochemistry of greisenized granites and metasomatic schists of tungsten-tin deposits in Portugal. In: Helgeson HC, ed. *Chemical Transport in Metasomatic Processes*. NATO ASI Series C218, pp. 681–700.
Neiva AMR, Silva MMVG, Gomes MEP. 2007. Crystal chemistry of tourmaline from Variscan granites, associated tin-tungsten- and gold deposits, and associated metamorphic and metasomatic rocks from northern Portugal. *Neues Jahrbuch für Mineralogie – Abhandlungen* 184(1): 45–76.
Noronha F, Doria A, Dubessy J, Charoy B. 1992. Characterization and timing of the different types of fluids present in the barren and ore-veins of the W-Sn deposit of Panasqueira, Central Portugal. *Mineralium Deposita* 27: 72–79. https://doi.org/10.1007/BF00196084.
Pearce N, Perkins W, Westgate J, Gorton M, Jackson S, Neal C, *et al*. 1997. A compilation of new and published major and trace element data for NIST SRM 610 and NIST SRM 612 glass reference materials. *Geostandards and Geoanalytical Research* 21: 115–144. https://doi.org/10.1111/j.1751-908X.1997.tb00538.x.
Petrus JA, Kamber BS. 2012. VizualAge: A Novel Approach to Laser Ablation ICP-MS U-Pb Geochronology Data Reduction. *Geostandards and Geoanalytical Research* 36: 247–270.
Philpotts JA, Schnetzler CC. 1970. Phenocryst-matrix partition coefficients for K, Rb, Sr and Ba, with applications to anorthosite and basalt genesis. *Geochimica et Cosmochimica Acta* 34: 307–322.
Pichavant M. 1981. An experimental study of the effect of boron on a water-saturated haplogranite at 1 Kbar vapour pressure. *Contributions to Mineralogy and Petrology* 76: 430–439.
Pichavant M, Villaros A, Deveaud S, Scaillet B, Lahlafi M. 2016. The Influence of Redox State On Mica Crystallization in Leucogranitic and Pegmatitic Liquids. *The Canadian Mineralogist* 54: 559–581. https://doi.org/10.3749/canmin.1500079.
Pirajno F. 1992. Greisen systems. In: *Hydrothermal Mineral Deposits*. Berlin, Heidelberg: Springer, pp. 280–324.
Pochon A, Poujol M, Gloaguen E, Branquet Y, Cagnard F, Gumiaux C, *et al*. 2016. U-Pb LA-ICP-MS dating of apatite in mafic rocks: Evidence for a major magmatic event at the Devonian-Carboniferous boundary in the Armorican Massif (France). *Am. Mineral.* 101: 2430–2442.
Pollard PJ, Taylor RG, Cuff C. 1988. Genetic Modelling of Greisen-Style Tin Systems. In: Hutchison CS, ed. *Geology of Tin Deposits in Asia and the Pacific*. Berlin, Heidelberg: Springer, pp 59–72.
Polya DA. 1989. Chemistry of the main-stage ore-forming fluids of the Panasqueira W-Cu-(Ag)-Sn deposit, Portugal: implications for models of ore genesis. *Econ. Geol.* 84: 1134–1152.
Polya DA, Foxford KA, Stuart F, Boyce A, Fallick AE. 2000. Evolution and paragenetic context of low δD hydrothermal fluids from the Panasqueira W-Sn deposit, Portugal: New evidence from microthermometric, stable isotope, noble gas and halogen analyses of primary fluid inclusions. Geochim. Cosmochim. Acta 64: 3357–3371.
Ribeiro RF. 2017. Gravimetric Modelling and Geological Interpretation of Argemela-Panasqueira Area. Upublished MSc thesis, Universidade do Porto.
Robb L. 2005. Introduction to Ore-forming Processes. Malden, MA: Blackwell Publishing, 373 p.
Rusk B, Reed M. 2002. Scanning electron microscope-cathodoluminescence analysis of quartz reveals complex growth histories in veins from the Butte porphyry copper deposit, Montana. *Geology* 30(8): 727–730.
Rusk B. 2012. Cathodoluminescent textures and trace elements in hydrothermal quartz. In Götze J, Möckel R, eds. *Quartz: Deposits, Mineralogy and Analytics*. Heidelberg, New York: Springer, pp. 307–329.
Sanderson DJ, Roberts S, Gumiel P, Greenfield C. 2008. Quantitative Analysis of Tin- and Tungsten-Bearing Sheeted Vein Systems. Economic Geology 103: 1043–1056. https://doi.org/10.2113/gsecongeo.103.5.1043.
Shcherba GN. 1970. Greisens. *Int Geol Rev* 12: 114–255.
Schoene B, Bowring SA. 2006. U-Pb systematics of the McClure Mountain syenite: Thermochronological constraints on the age of the 40Ar/39Ar standard MMhb. *Contributions to Mineralogy and Petrology* 151: 615–630.
Smith MP, Banks DA, Yardley BWD. 1996. Fluid inclusion and stable isotope constraints on the genesis of the Cligga Head Sn-W deposit, SW England. *Eur J Mineral* 8: 961–974.
Snee LW, Sutter JF, Kelly WC. 1988. Thermochronology of economic mineral deposits; dating the stages of mineralization at Panasqueira, Portugal, by highprecision 40Ar/39Ar age spectrum techniques on muscovite. *Econ Geol* 83: 335–354.
Speer JA. 1984. Micas in igneous rocks. In: Bailey SW, ed. *Micas*. *Reviews in Mineralogy*, Vol. 13. Washington D.C.: Mineralogical Society of America, pp. 299–356.

Stemprok M. 1987. Greisenization (a review). Geol Rundsch, Springer-Verlag 76: 169.

Stemprok M, Pivec E, Langrova A. 2005. The petrogenesis of a wolframitebearing greisen in the Vykmanov granite stock, Western Krušné hory pluton (Czech Republic). *Bulletin of Geosciences* 80 (3): 163–184.

Tartèse R, Ruffet G, Poujol M, Boulvais P, Ireland TR. 2011. Simultaneous resetting of the muscovite K-Ar and monazite U-Pb geochronometers: a story of fluids. *Terra Nova* 23: 390–398.

Taylor RG. 1979. Geology of tin deposits. *Developments in Economic Geology, Elsevier*, 11: 543.

Taylor RG, Pollard PJ. 1988. Pervasive hydrothermal alteration in tin-bearing granite and implications for the evolution of ore-bearing magmatic fluids. *Canadian Institute of Mining and Metallurgy Special* 39: 86–95.

Thadeu D. 1951. Geologia do couto mineiro da Panasqueira. *Comunic Serv Geol Port* 32: 5–64.

Thomas JB, Watson EB, Spear FS, Shemella PT, Nayak SK, *et al*. 2010. TitaniQ under pressure: the effect of pressure and temperature on the solubility of Ti in quartz. *Contributions to Mineralogy and Petrology* 160: 743–759.

Tischendorf G, Gottesmann B, Förster H-J., Trumbull RB. 1997. On Li-bearing micas: estimating Li from electron microprobe analyses and an improved diagram for graphical representation. *Mineral. Mag.* 61: 809–834. https://doi.org/10.1180/min-mag.1997.061.409.05.

Tuttle OF, Bowen NL. 1958 Origin of Granite in the Light of Experimental Studies in the System $NaAlSi_3O_8$-$KAlSi_3O_8$-SiO_2-H_2O. *Geological Society of America*. https://doi.org/10.1130/MEM74.

Van Daele J, Hulsbosch N, Dewaele S, Boiron MC, Piessens K, Boyce A. 2018. Mixing of magmatic-hydrothermal and metamorphic fluids and the origin of peribatholitic Sn vein-type deposits in Rwanda. *Ore Geology Reviews.* 101. https://doi.org/10.1016/j.oregeorev.2018.07.020.

Vilas L, de San Jose MA, Garcia-Hidalgo JF, Herranz P, Pelaez JR, Perejon A, *et al*. 1990. Autochthonous Sequences. In Dallmeyer RD, Garcia EM, eds. *Pre-Mesozoic Geology of Iberia, IGCP-Project 233*. Berlin, Heidelberg: Springer, pp. 145–219. https://doi.org/10.1007/978-3-642-83980-1_14.

Villaseca C, Merino E, Oyarzun R, Orejana D, Pérez-Soba C, Chicharro E. 2014. Contrasting chemical and isotopic signatures from Neoproterozoic metasedimentary rocks in the Central Iberian Zone (Spain) of pre-Variscan Europe: Implications for terrane analysis and Early Ordovician magmatic belts. *Precambrian Research* 245: 131–145. https://doi.org/10.1016/j.precamres.2014.02.006.

Wark DA, Watson EB. 2006. TitaniQ: a titanium-in-quartz geothermometer. *Contributions to Mineralogy and Petrology* 152: 743–754.

Weil JA. 1984. A review of electron spin spectroscopy and its application to the study of paramagnetic defects in crystalline quartz. *Physics and Chemistry of Minerals* 10: 149–165.

Werner ABT, Sinclair WD, Amey EB. 2014. International strategic mineral issues summary report—Tungsten (ver. 1.1, November 2014). U.S. Geological Survey Circular 930-O, 74 p.

Wheeler A. 2015. Technical report on the mineral resources and reserves of the Panasqueira mine, Portugal. Report NI 43-101, Prepared for Almonty Industries.

White RW, Powell R, Holland TJB. 2007. Progress relating to calculation of partial melting equilibria for metapelites. *Journal of Metamorphic Geology* 25: 511–527.

Whitney DL, Evans BW. 2010. Abbreviations for names of rock-forming minerals. *Am. Mineral* 95: 185–187.

Winderbaum L, Ciobanu CL, Cook NJ, Paul M, Metcalfe A, Gilbert S. 2012. Multivariate analysis of an LA-ICP-MS trace element dataset for pyrite. *Math. Geosci.* 44: 823–842.

Zimmer K, Zhang YL, Lu P, Chen YY, Zhang GR, Dalkilic M, *et al*. 2016. SUPCRTBL: A revised and extended thermodynamic dataset and software package of SUPCRT92. *Computer and Geosciences* 90: 97–111.

Cite this article as: Launay G, Sizaret S, Lach P, Melleton J, Gloaguen E, Poujol M. 2021. Genetic relationship between greisenization and Sn-W mineralizations in vein and greisen deposits: Insights from the Panasqueira deposit (Portugal), *BSGF - Earth Sciences Bulletin* 192: 2.